Propagation of Beta/Gamma Rhythms in the Cortico-Basal Ganglia Circuits of the Parkinsonian Rat

Timothy O. West[1,2*], Luc Berthouze[3,4], David M. Halliday[5], Vladimir Litvak[2], Andrew Sharott[6], Peter J. Magill[6,7], Simon F. Farmer[8,9]

[1]*CoMPLEX, Centre for Mathematics and Physics in the Life Sciences and Experimental Biology, UCL Department of Physics and Astronomy, Gower Street, London, WC1E 6BT*

[2]*Wellcome Trust Centre for Neuroimaging, UCL Institute of Neurology, Queen Square, London, WC1N 3BG*

[3]*Centre for Computational Neuroscience and Robotics, University of Sussex, Falmer, UK*

[4]*UCL Great Ormond Street Institute of Child Health, Guildford St., London, WC1N 1EH*

[5]*Department of Electronic Engineering, University of York, YO10 5DD, UK.*

[6]*Medical Research Council Brain Network Dynamics Unit, University of Oxford, Oxford, OX1 3TH, United Kingdom.*

[7]*Oxford Parkinson's Disease Centre, University of Oxford, Oxford OX1 3QX, United Kingdom.*

[8]*Department of Neurology, National Hospital for Neurology & Neurosurgery, Queen Square, London WC1N 3BG*

[9]*Sobell Department of Motor Neuroscience and Movement Disorders, Institute of Neurology, UCL, London WC1N 3BG.*

**Corresponding Author*

Abstract

Much of the motor impairment associated with Parkinson's disease is thought to arise from pathological activity in the networks formed by the basal ganglia (BG) and motor cortex. To evaluate several hypotheses proposed to explain the emergence of pathological oscillations in Parkinsonism, we investigated changes to the directed connectivity in BG networks following dopamine depletion. We

recorded local field potentials (LFPs) in the cortex and basal ganglia of rats rendered Parkinsonian by injection of 6-hydroxydopamine (6-OHDA) and in dopamine-intact controls. We performed systematic analyses of the networks using a novel tool for estimation of directed interactions (Non-Parametric Directionality, NPD). Additionally, we used a 'conditioned' version of the NPD analysis which reveals the dependence of the correlation between two signals upon a third reference signal. We find evidence of the dopamine dependency of both low beta (14-20 Hz) and high beta/low gamma (20-40 Hz) directed interactions within the network. Notably, 6-OHDA lesions were associated with enhancement of the cortical "hyper-direct" connection to the subthalamic nucleus (STN) and its feedback to the cortex and striatum. We find that pathological beta synchronization resulting from 6-OHDA lesioning is widely distributed across the network and cannot be located to any individual structure. Further, we provide evidence that high beta/gamma oscillations propagate through the striatum in a pathway that is independent of STN. Rhythms at high beta/gamma show susceptibility to conditioning that indicates a hierarchical organization when compared to low beta. These results further inform our understanding of the substrates for pathological rhythms in salient brain networks in Parkinsonism.

Keywords

Parkinson's disease; basal ganglia; local field potential; synchronization; connectivity;

New & Noteworthy

We present a novel analysis of electrophysiological recordings in the cortico-basal ganglia network with the aim of evaluating several hypotheses concerning the origins of abnormal brain rhythms associated with Parkinson's disease. We present evidence for changes in the directed connections within the network following chronic dopamine depletion in rodents. These findings speak to the plausibility of a "short-circuiting" of the network that gives rise to the conditions from which pathological synchronization may arise.

Introduction

The basal ganglia (BG) are host to a small but important cluster of dopaminergic neurons that act to modulate the activity of a large re-entrant network that comprises the cortico-basal ganglia-thalamo-cortical circuit (DeLong and Wichmann 2010; Lanciego et al. 2012). Investigation of the structure of this network (Smith et al. 1998; Bolam et al. 2000) has led to what has become a canonical view of the circuit (depicted in Figure 1A) and has formed the basis from which a number of process theories of BG function have arisen (for a review, see Schroll and Hamker, (2013)).

Recent theory concerning the organisation of brain networks and communication within them via synchronized oscillations (Varela et al. 2001; Fries 2005, 2015; Bressler and Menon 2010; Thut et al. 2012) has emphasised the importance of understanding the dynamics of these networks beyond that afforded by studying structural connectivity alone (Deco et al. 2008, 2012). Neural oscillations and their

synchronization have been measured across multiple spatial scales of brain activity, from single neuronal discharges up to the level of mesoscale neural ensembles such as those measured in the local field potential (LFP) or electrocorticogram (ECoG). Moreover, dysregulations of oscillations and inter-areal synchrony have been reported in brain disorders such as Parkinson's disease (PD), schizophrenia, and epilepsy, leading to the hypothesis that the oscillations themselves bear a causal role in the behavioral impairments associated with these pathologies (Schnitzler and Gross 2005; Uhlhaas and Singer 2006; Hammond et al. 2007).

Excessive beta oscillations (14-30 Hz) in the BG associated with dopamine depletion have been observed reliably in untreated patients with PD (Levy et al. 2000; Brown et al. 2001; Weinberger et al. 2006; Hammond et al. 2007). Beta rhythms are attenuated by treatments such as dopamine replacement therapy (Kühn et al. 2006; Weinberger et al. 2006; West et al. 2016; Beudel et al. 2017; Levy 2002) and deep brain stimulation (DBS) (Ray et al. 2008; Eusebio et al. 2011; Whitmer et al. 2012) in a way that correlates with the degree of improvement of akinetic/rigid motor symptoms. This has strengthened the argument that the pathological beta rhythms are directly related to the functional impairment seen in patients (Hanslmayr et al. 2012; Brittain and Brown 2014). Furthermore, gamma activity in the motor system has been hypothesized to be prokinetic (Schoffelen et al. 2005). In PD, the spectral power of multiunit recordings from STN at 40-90 Hz have been demonstrated to be negatively correlated with bradykinetic symptoms in patients (Sharott et al. 2014).

The pathological oscillations observed in mesoscale electrophysiological signals are a direct consequence of changes to the underlying networks of neuronal ensembles that generate them. This understanding has led to the re-classification of multiple neurological diseases such as PD or Tourette's as 'circuit disorders' (DeLong and Wichmann 2010). Knowledge of how dopamine depletion results in changes to the network, and the subsequent emergence of pathological synchrony is likely to lead to a better understanding of the causes of impairment and its treatments (Shen et al. 2008; Schroll et al. 2014). Thus, improving insight into how changes network organization leads to the emergence of pathological dynamics is an important line of enquiry (Wichmann and DeLong 1999; Dostrovsky and Bergman 2004; Holgado et al. 2010)

Previous work aiming to understand the origins of the pathological beta rhythm has involved systematic lesioning of the BG network (Ni et al. 2000; Tachibana et al. 2011), computational modelling (Holgado et al. 2010; Moran et al. 2011; Marreiros et al. 2013; Nevado-Holgado et al. 2014; Pavlides et al. 2015; Lienard et al. 2017), and techniques from signal analysis (Sharott et al. 2005a; Mallet et al. 2008a, 2008b; Litvak et al. 2011a). In this paper, we take the latter approach and, through analysis of neural recordings, aim to infer the changes in neural transmission that occur in cortico-BG circuits following chronic dopamine depletion.

Connectivity between parts of the brain can be inferred from the statistical dependencies that arise due to neural transmission: we refer to this as functional connectivity as per Friston (2011). Previous studies have aimed to describe 'effective' connectivity (i.e. causal interactions) within this network and have employed the dynamic causal modeling (DCM) framework in order to do so. To date, two such studies have utilised the inversion of biophysical models upon cross spectral densities from recordings in either anaesthetised 6-OHDA lesioned rats (Moran et al. 2011), or awake DBS patients (Marreiros et al. 2013). Both found evidence for the strengthening of the cortico-subthalamic connection (termed the 'hyper-direct' pathway (Nambu et al. 2002)) in the dopamine-depleted state.

From this work amongst others, several hypotheses have arisen concerning the emergence of pathological beta rhythms as a result of the dopamine depletion associated with PD (for a review see Holgado et al. 2010). These include the dopamine-dependent modulation of recurrent loops within the network, either between the reciprocally-coupled network of neurons of the subthalamic nucleus (STN) and the external globus pallidus (GPe) (Plenz and Kital 1999; Bevan et al. 2002; Terman et al. 2002; Holgado et al. 2010; Liu et al. 2017); or of a longer loop involving feedback from BG output nuclei to the cortex via thalamo-cortical tracts (Leblois et al. 2006; Pavlides et al. 2012, 2015). Alternatively, it has been proposed that dopamine depletion disrupts mechanisms which regulate the gain of cortical afferents to the BG and somehow disrupt striatal outflow (Brown 2007; Hammond et al. 2007). The striatum (STR) itself has also been implicated in the generation of pathological beta rhythms, either through alterations to its internal dynamics (McCarthy et al. 2011; Damodaran et al. 2015); or via increased striatal inhibition of targets in the GPe that act to promote beta synchrony (Gillies and Willshaw 2004; Kumar et al. 2011a).

Here, using a recently described non-parametric (model-free) signal analysis technique (Halliday et al., 2015), we study the effects of dopamine depletion upon neural connectivity in the network formed by elements of the BG and motor cortex in 6-OHDA-lesioned and dopamine-intact control rats. We employ this method as a measure of *directed* functional connectivity (hereon shortened to directed connectivity). It is a model-free estimate that makes no assumptions as to the causes of the data (for discussion see Bastos and Schoffelen 2016), only that temporal precedence implies a driving neuronal influence (please see later sections for discussion). Furthermore, we use a a multivariate extension of the framework (Halliday et al. 2016) in order to determine whether the interaction between two areas shares correlation with activity recorded at a third structure in the network. This approach provides insight into frequency-specific directional connectivity and the degree to which transmission between two coupled regions are autonomous of another reference region. By recording LFPs and ECoG in 6-OHDA–lesioned animals and dopamine-intact controls we aim to identify changes to connectivity that occur as a result of the loss of dopamine from these circuits. Our findings are interpreted within the context of the canonical circuit (Figure 1A), as well as other existing models of basal ganglia

connectivity, and several hypotheses concerning the generation and propagation neural rhythms in the network.

Methods

Experimental Data

Electrophysiological Recordings

Experimental procedures were carried out on adult male Sprague-Dawley rats (Charles River, Margate, UK) and were conducted in accordance with the Animals (Scientific Procedures) Act, 1986 (UK). Recordings were made in eight dopamine-intact control rats (288–412 g) and nine 6-OHDA-lesioned rats (285– 428 g at the time of recording), as described previously (Magill et al. 2006; Mallet et al. 2008a, 2008b; Moran et al. 2011). Briefly, anesthesia was induced with 4% v/v isoflurane (Isoflo, Schering-Plough Ltd., Welwyn Garden City, UK) in O2, and maintained with urethane (1.3 g/kg, i.p.; ethyl carbamate, Sigma, Poole, UK), and supplemental doses of ketamine (30 mg/kg; Ketaset, Willows Francis, Crawley, UK) and xylazine (3 mg/kg; Rompun, Bayer, Germany).

The ECoG was recorded via a 1 mm diameter steel screw juxtaposed to the dura mater above the right frontal cortex (centred at 4.5 mm anterior and 2.0 mm lateral of Bregma, corresponding to the "secondary motor cortex" (M2) of (Paxinos and Watson 2007) or the medial agranular field of the somatic sensorimotor cortex of Donoghue and Wise, (1982); see Figure 1B) and was referenced against another screw implanted in the skull above the ipsilateral cerebellar hemisphere. Raw ECoG was band-pass filtered (0.3–1500 Hz, -3 dB limits) and amplified (2000x; DPA-2FS filter/amplifier: Scientifica Ltd., Harpenden, UK) before acquisition (see below). Extracellular recordings of LFPs in the dorsal striatum (STR), GPe and STN were simultaneously made in each animal using 'silicon probes' (NeuroNexus Technologies, Ann Arbor, MI); a first probe captured LFPs in STR and GPe, whereas a second probe captured LFPs in the STN (Figure 1B). Each probe had one vertical array of 16 recording contacts (impedance of 0.9–1.3 MΩ measured at 1000 Hz; area of ~400μm^2), and each contact on a given probe was separated by 100 μm. Recording sites in the BG were verified by post hoc histology, as described previously (Magill et al. 2006; Mallet et al. 2008a, 2008b), as well as by comparisons of recorded unit activity with the characteristic discharges of STR, GPe and STN neurons in anesthetized dopamine-intact rats and 6-OHDA-lesioned rats (Magill et al. 2006; Mallet et al. 2008a, 2008b; Abdi et al. 2015; Sharott et al. 2017).The same two probes were used throughout these experiments, but were cleaned after each experiment in a proteolytic enzyme solution to ensure that contact impedances and recording performance were not altered by probe use and re-use (Magill et al. 2006; Sharott et al. 2017). Monopolar probe signals were recorded using high-impedance unity-gain operational amplifiers (Advanced LinCMOS: Texas Instruments, Dallas, TX) and were referenced against a screw implanted above the contralateral cerebellar hemisphere. After initial amplification, extracellular signals were further amplified (1000x) and low-pass filtered at 6000 Hz using programmable differential amplifiers

(Lynx-8: Neuralynx, Tucson, AZ). The ECoG and probe signals were each sampled at 17.9 kHz using a single Power1401 Analog-Digital converter (with integrated ADC16 expansion units) and a PC running Spike2 acquisition and analysis software (Cambridge Electronic Design Ltd., Cambridge, UK). All signals recorded in a given experimental epoch were captured in a single data file. This, together with the use of a fixed/consistent sampling rate and a single acquisition interface, ensured accurate synchronization (temporal alignment) of cortical and BG signals.

Neuronal activity was recorded during episodes of spontaneous 'cortical activation', which contain patterns of activity that are similar to those observed during the awake, behaving state (Steriade 2000). Cortical activation was defined according to ECoG activity. Neuronal activity patterns present under this anesthetic regime may only be qualitatively similar to those present in the unanesthetized brain. However, the urethane-anesthetized animal still serves as a useful model for assessing ensemble dynamics within the basal ganglia. Indeed, in 6-OHDA-lesioned animals, exaggerated beta oscillations emerge in cortico-basal ganglia circuits during activated brain states thus accurately mimicking the oscillatory activity recorded in awake, un-medicated PD patients. Examples of the raw electrophysiological signals as well the corresponding power spectra for control and lesioned animals are shown in Figure 2.

6-Hydroxydopamine Lesions of Dopamine Neurons

Unilateral 6-OHDA lesions were carried out on 200–250 g rats, as described previously (Mallet et al. 2008a, 2008b). Twenty-five minutes before the injection of 6-OHDA, all animals received a bolus of desipramine (25 mg/kg, i.p.; Sigma) to minimize the uptake of 6-OHDA by noradrenergic neurons (Schwarting and Huston 1996a). Anesthesia was induced and maintained with 4% v/v isoflurane (see above). The neurotoxin 6-OHDA (hydrochloride salt; Sigma) was dissolved immediately before use in ice-cold 0.9% w/v NaCl solution containing 0.02% w/v ascorbate to a final concentration of 4 mg/ml. Then 3 ml of 6-OHDA solution was injected into the region adjacent to the medial substantia nigra (4.5 mm posterior and 1.2 mm lateral of Bregma, and 7.9 mm ventral to the dura. The extent of the dopamine lesion was assessed 14–16 days after 6-OHDA injection by challenge with apomorphine (0.05 mg/kg, s.c.; Sigma) (Schwarting and Huston 1996b). The lesion was considered successful in those animals that made >80 net contraversive rotations in 20 min. Electrophysiological recordings were carried out ipsilateral to 6-OHDA lesions in anesthetized rats 21–42 days after surgery, when pathophysiological changes in the basal ganglia are likely to have levelled out near their maxima (Mallet et al. 2008a).

Data Acquisition and Analysis

Data Conversion and Pre-Processing

To isolate LFPs and ECoGs, all electrophysiological data were down-sampled from a hardware native 17.9 kHz to 250 Hz using Spike2 acquisition and analysis software (version 4; Cambridge Electronic Design Ltd., Cambridge, UK). Data were then imported from Spike2 into MATLAB (The Mathworks,

Nantucket, MA, USA) where they were analysed using custom scripts utilizing routines from the Fieldtrip software package (contained within SPM 12.3) (Oostenveld et al. 2011; http://www.fieldtriptoolbox.org/), as well as Neurospec (http://www.neurospec.org/). Data were pre-processed as follows: i) data were first truncated to remove 1 second from either end of the recording, ii) mean subtracted; iii) band-passed filtered with a finite impulse response, two-pass (zero-lag) filter designed such that the filter order is rounded to the number of samples for 3 periods of the lowest frequency, between 4-100 Hz; iv) data were then split into 1 second epochs; v) each epoch was subjected to a Z-score threshold criterion such that epochs containing any high amplitude artefacts were removed. Examples of outcomes from this pre-processing are shown in figure 2. All ECoG/LFP time series were 90-100 seconds in duration.

Analyses of Neurophysiological Signals

Estimates of Spectral Power

Power analyses were made using the averaged periodogram method across 1 second epochs and using a Hanning taper to reduce the effects of spectral leakage. Frequencies between 49-51 Hz were removed so that there was no contribution from 50 Hz line noise. The sampling rate of 250 Hz gives a Nyquist frequency of 125 Hz and 1 second epochs yield Fourier spectra with a 1 Hz frequency resolution and a periodogram resulting from an average of ~100 spectra per channel. All analyses were made using the Neurospec toolbox. Individual spectra were normalized for group level comparisons by dividing by the total power in the range 4-48 Hz.

Non-zero Phase Lag Functional Connectivity Analysis: Imaginary Coherence

The commonly used spectral coherence (Halliday et al. 1995) is sensitive to spurious correlations resulting from instantaneous volume conduction between the two signals of interest (Bastos and Schoffelen, 2016). This issue is of the most concern when recordings are made in close spatial proximity such as that made by adjacent contacts on the silicon probes used in these experiments. In order to circumvent this issue, several methods have been developed such as taking the imaginary part of coherence (Nolte et al. 2004), the phase lag index (PLI) (Stam et al. 2007), or the weighted phase lag index (Vinck et al. 2011). For this study, we used initially the simplest method - the imaginary coherence (iCOH) that is derived from the complex coherency. The more often used coherence is the magnitude-squared coherency. Coherence is real valued on a scale between 0-1, with 1 indicating maximal correlation between two signals and 0 indicating an absence of correlation (Halliday et al., 1995). Nolte and co-workers have suggested that by taking the imaginary part of the coherency, the contribution of correlations with zero phase lag (that is having only a real component) can be negated. This property is shared with the non-parametric directionality analysis that we will later introduce for estimates of directed connectivity. We note the concerns in Stam et al. (2007) on the validity of imaginary coherence analysis and so include additional analyses based on non-parametric directionality

and use the iCOH metric as a first-pass demonstration that non-zero phase lag interactions are present in the data.

Non-Parametric Directionality

Estimates of directed connectivity were computed using non-parametric directionality (NPD) which is a novel framework to decompose classical, non-parametric Fourier-based, coherence estimates by direction (Halliday, 2015). Coherence between two random processes, or random signals, is defined as the ratio of the magnitude squared cross spectrum between the two signals to the product of their auto spectra. It is difficult to infer any directionality from this ratio involving cross spectra and auto-spectra. The approach introduced in Halliday (2015) uses optimal Minimum Mean Square Error (MMSE) pre-whitening of the two signals such that the coherence is calculated from the cross-spectrum only, as the denominator becomes equal to 1. Pre-whitening refers to the process of filtering a signal prior to spectral analysis to make its frequency content closer to white noise.

The pre-whitening step generates two new random processes which have spectra equal to 1 at all frequencies, and which have the same coherence as the two original signals. The coherence between the pre-whitened signals is calculated only from the cross spectrum between the pre-whitened processes and this is identical to the original coherence. From this MMSE pre-whitened cross spectrum an inverse Fourier transform generates a time domain correlation measure. This is analogous to the approach used to generate a standard cross-covariance estimate in the time domain, except the MMSE pre-whitened time domain correlation measure only has features that occur as a result of the correlation between the signals, effectively removing the confounding influence of the original signals' autocorrelation.

Three quantities are extracted from this time domain correlation measure according to time lag. These are components with negative time lags, the value at zero-time lag, and components at positive time lags. These are used to calculate the strength of correlation in the reverse, zero-lag and forward directions respectively. Three inverse Fourier transforms, using the sections over these three lags ranges, are used to obtain the reverse, zero-lag, and forward components of the original coherence estimate. These provide a summative decomposition of the original non-parametric coherence at each frequency into reverse, zero-lag and forward components.

In this study the zero-lag component is assumed to reflect volume conduction. The forward and reverse components of coherence are used to infer directionality between the different regions. For example, STN activity lagging M2 activity results in a significant forward component of coherence between M2 and STN (with M2 as reference), whereas STN activity leading M2 activity results in a significant reverse component of coherence.

The concept of partial coherence is well established (Rosenberg et al., 1998; Medkour et al. 2009), where coherence is conditioned on a third signal. This conditioning takes the form of a simple linear regression in the frequency domain of each of the two original signals on the third signal or predictor.

The resulting partial coherence estimates can be used to test the hypothesis that the pairwise correlation between the original signals can be accounted for by the third signal. The NPD framework is extended to decompose partial coherence into directional components in Halliday et al (2016). The analysis decomposes the partial coherence into the same three directional components: forward, reverse and zero-lag. The approach is similar to the bivariate case, except MMSE pre-whitening is applied using partial auto-spectra and the partial cross spectrum.

This analysis can indicate if the signals reflected in the correlation are common to other parts of the network. For example, the partial correlation between A and B with C as predictor can be used to determine if the flow of information from A → B is independent of area C, or whether the flow of information is A → C → B, in which case the partial coherence between A and B with C as predictor should be zero. The partial coherence can also be used to investigate if the flow of information is C → A and C → B, or if it is A → B → C or C → A → B, which for the latter case the partial coherence, and any directional components should be zero.

This assumes that the conditioning signal, C, is representative of the activity in the relevant brain area. If the signal, C, only captures part of the activity in the brain area then the partial coherence estimate may still have residual features. The most robust interpretation of the partial coherence and multivariate non-parametric directionality is where the partial coherence (and any directional components) are not significant compared to the directional components for the ordinary coherence. It must be noted that these methods are useful in detecting the linear coupling (additive mixing/linear correlation) of signals. NPD is not suited for detection of non-linear interactions between signals such as cross-frequency coupling for instance.

Statistics and Visualization

In order to make statistical comparisons of power, connectivity and directionality spectra between lesioned and control recordings we used cluster based permutation testing (Maris and Oostenveld 2007) which avoids introducing bias through the prior specification of frequency bands. Briefly, the method computes multiple independent t-statistics for each sample (channel-frequency pair) between the two experimental conditions (lesion and control). We assume that in regions of the spectra where there is a true physiological difference in the distributions of a metric of interest (i.e. power, iCOH, NPD) there will be a high value of the t-statistic in several adjacent frequency bins and this group of neighbouring bins is called ‘a cluster’.

The purpose of the cluster-based permutation test is to find clusters which are ‘heavier’ (i.e. have a greater sum of t-statistic values in the cluster) than could be expected under the null hypothesis. Candidate clusters to be tested are identified by setting a threshold on the t-statistic. Importantly, this cluster-forming threshold does not affect the false alarm rate of the test, only the sensitivity to large clusters with smaller t-values as opposed to small clusters with large t-values. The statistical

significance of candidate clusters is then tested by approximating the reference distribution using a large number of permutations where the condition labels are randomly reassigned and the whole procedure of cluster identification is repeated. The clusters in the original data are then compared to the top tail of the reference distribution according to the pre-defined statistical threshold (typically, 5%). The permutation testing requires no assumption of normality and affords a correction for the multiple comparison problem by controlling the family-wise error rate. For full details of the method, see Maris (2012).

The cluster-forming threshold was $p<0.05$ and the permutation test threshold was set at $p<0.025$ (as it is a two-sided test). The number of permutations was set to 5000 which tenders a lowest possible P-value equal to 0.0004. Cluster statistics were computed using the '*ft_freqstatistics*' routine in the Fieldtrip toolbox. For testing of the effect of conditioning upon the NPD estimate, statistics are computed identically as described above, but treating the conditioned and unconditioned spectra as the two experimental conditions of interest. As each animal contained multiple recordings per subcortical site we averaged the spectra from these recordings into a subject mean. Group level plots indicate the group mean in bold ±1 standard error of the mean (S.E.M.).

Results

Spectral Power

Examples of spectra computed from LFP and ECoG signals recorded in individual animals can be seen in figure 2 (B and D). All the 6-OHDA-lesioned rats demonstrated a clear peak in the spectra in the range 18-22 Hz (encompassing low beta/lower end of high beta frequencies) for LFP recordings across all subcortical recording sites as well as for the sensorimotor ECoGs. In some animals, cortical beta was weaker than that observed subcortically. None of the LFP data from control animals contained beta peaks in the spectra although some (4 of 8) showed a wide, low amplitude peak around 20-40 Hz that was clearly above the 1/f background and most prominent in the recordings at M2 (an example of which is seen in figure 2B). Analysis of the group averaged spectra (figure 3) shows that the beta peak is significantly increased in the dopamine-depleted animals**.** Cluster-based permutation testing demonstrated significant differences in group level spectra between control and lesion conditions with clusters showing increases in power associated with dopamine depletion in the M2 (16-23 Hz, P=0.001), STR (18-21 Hz, P=0.011), STN (16-21 Hz, P=0.012), and GPe (17-22 Hz, P=0.008). No differences between lesioned and control animals were found for frequencies >22 Hz in any structures.

Functional Connectivity: Imaginary Coherence (iCOH)

Initial analyses of connectivity of the recorded LFPs using magnitude squared coherence showed large magnitude (>0.9) wideband (0 - 60Hz) coherences that were indicative of a large field spread effect (data not shown). This was most apparent in subcortical-subcortical analyses but was also detected for

cortical-subcortical pairings. To estimate coherence avoiding contamination by volume conduction we opted to calculate non-zero phase lag correlations using the imaginary part of coherence (iCOH) (see figure 4).

We found that activity in the low beta range (14-20 Hz) associated with 6-OHDA dopamine depletion is spread diffusely across the network with all inter-regional comparisons showing a significant beta peak in the iCOH spectrum. Notably, the strongest coherence in the low beta band involved STN, with STN/STR and STN/GPe pairs both showing coefficients greater than 0.2. Within region connectivity (i.e. STN contact 1 to contact 2) was found to be present in this frequency range for only recordings within STN or GPe, where there is a clear beta peak. No within region connectivity was found in the STR where the iCOH spectra were flat.

Analysis of statistical differences using the cluster based permutation testing between control and lesioned animals showed significant increases of iCOH in the beta band in the lesioned animals and for 5/10 LFP pairs tested: STN/STR (14-21 Hz, P=0.006), STN/STN (19-25 Hz, P = 0.014), GPe/STR (14-16 Hz, P = 0.010), GPe/STN (14-21 Hz, P=0.006), and GPe/GPe (19-23 Hz, P=0.004). Notably, no pairs involving M2 showed significant modulation of beta-band activity following dopamine depletion when tested using cluster statistics. Taken generally, these results are indicative of widespread, non-zero lag, low beta-band connectivity across the entire cortico-BG network that is increased in the dopamine-depleted rats.

In the control rats, connectivity in the beta range was reduced relative to the dopamine depleted rats. Instead, there was wide-band iCOH in the high beta/low gamma bands, ranging from 20 Hz to 50 Hz in most cases but up to 70 Hz for the STN/M2 interactions. The majority of gamma band interactions where iCOH was high (> 0.2) were found in connections involving the STN. Additionally, iCOH in these bands is evident between GPe/M2 and GPe/STR although this was weaker (at around ~0.1) than connections analysed with pairs involving the STN. iCOH in these bands is present in both the lesioned and control animals and does not show a strong modulation by dopamine as evidenced by the lack of significant clusters in the permutation tests for these bands. The iCOH analyses present evidence for strong non-zero coherences at these frequencies even when spectral power at these frequencies is small. It must be noted that there exists a separation between analyses of rhythmicity and correlation of rhythmic activity that are complimentary properties of the signals.

Non-parametric Directionality (NPD)

We next investigated directed connectivity between recorded regions. The results of the analysis using the NPD measure are presented in figure 5. The iCOH and the sum of the non-instantaneous parts (forward and backward) of the NPD are similar, and both methods revealed similar patterns of connectivity (data not shown). Analysis of the instantaneous (zero-lag) NPD in isolation demonstrated the existence of high amplitude, wide-band interactions that were similar to those found with magnitude

squared coherence (data not shown), and are likely due to zero-phase field spread of activity between recordings. Analyses of directional interactions of the LFPs and ECoG hereon will use the forward and backward components of the NPD to discern directional connectivity between LFPs recorded from each brain structure.

We observed that directional interactions of low beta-band activity in the dopamine depleted animals predominate in the direction leading from M2 and that they descend the hierarchy of the BG. Interestingly we noted a significant difference in the cortical-subthalamic beta band interaction between lesioned and control animals only in the feedback connection STN → M2 (16-18 Hz, P=0.020), which would suggest that STN feedback to M2 is strengthened in the dopamine depleted state. In the case of the STN/GPe circuit, and unlike iCOH, the non-instantaneous components of NPD do not show 6-OHDA related increases in beta coupling in either direction for the lesioned rats. Rather, NPD suggests a directional asymmetry in activity in the high beta/gamma band with forward connections from GPe → STN connection stronger than in the reverse direction (cluster statistics testing differences between forward and backward spectra in the 6-OHDA recordings: 4-43 Hz, P<0.001). Notably, we see a feedback in the STN → STR that is most prominent in the lesion condition, a feature that will be relevant with respect to results discussed later.

The pattern of activity in the high beta/gamma range between cortical and subcortical regions appeared to be principally cortically leading with the coefficient of the interactions in the 20-40 Hz range being up to 2/3 larger in the dopamine-intact control rats (top row of figure 5). Cluster-based permutation analysis showed a significant increase in the high/gamma M2 → GPe NPD in the control vs the lesion condition (25-30 Hz, P=0.020). High beta/gamma connections from subcortical structures feeding back to M2, are weaker than the cortically leading connections, but are still present for striatal and globus pallidus feedback to M2 (first column, row 2 and 4, figure 5). Again, there was a clear peak in the high beta NPD from STN→ STR in the lesioned animals, although a dependence on dopamine was not seen to be significant when testing with cluster statistics. The finding of a large NPD interaction from STN to STR does not accord with the canonical circuit (Figure 1A) but may instead imply feedback to striatum via subcortical thalamo-striatal loops that will be discussed in a later section of this paper.

Inferring Routing of Brain Rhythms: Partialized Non-Parametric Directionality

We repeated the NPD analysis as before but this time by systematically partialising out (conditioning) the contribution made by LFPs/ECoG recorded from each brain structure to the bivariate analyses presented in the previous section of the results. We again employed cluster statistics to determine significant differences between the non-conditioned NPD spectra and its conditioned variant shown in this section of the results.

Conditioning the NPD using Local Field Potentials Recorded from the STN

We first conducted a partialisation (conditioning) of the NPD estimate using LFPs recorded from within the STN (figure 6). Conditioning with signals from the STN does not remove beta connectivity between the remaining structures in the network although it does weaken the majority of comparisons in the control (6 of 6 comparisons, red bars) but not the lesion (2 of 6 comparisons, blue bars) animals (see figure 6, red and blue bars respectively). Cluster statistics indicate that the following NPDs for the control experiments were significantly reduced by conditioning with the STN signal: M2 → STR (14-33 Hz, $P<0.001$), M2 → GPe (14-33 Hz, $P<0.001$; 37-49 Hz, $P=0.008$), STR → GPe (10-49 Hz, $P<0.001$), GPe → STR (18-49 Hz, $P<0.001$) as well as feedback connections (returning to cortex): STR → M2 (14-27 Hz, $P<0.001$), GPe → M2 (18-49 Hz, $P<0.001$). Furthermore, conditioning the NPD with the signal from STN does not disrupt the 6-OHDA associated increases of M2 input to either the STR (14-21 Hz, $P<0.001$) or GPe (14-21 Hz, $P<0.001$) (black bars). We also found in the dopamine-depleted state that there was increased (relative to the controls) feedback to M2 from both GPe (16-20 Hz, $P=0.016$) and STR (16-20 Hz, $P=0.006$).

Notably we observed some separation in the effects of the conditioning between the control and lesion experiments. In the control animals conditioning the NPD on LFPs recorded at STN acted to reduce activity in a wide band (~12-40 Hz) for the forward connections (propagating down the indirect pathway; i.e. M2 → STR, M2 → GPe, and STR → GPe), whilst the return connections (STR → M2, and GPe → M2) were only affected by conditioning at a tighter band corresponding to low beta. This would suggest that in the healthy animal signals returning to cortex via STN occur at low beta frequencies. Lesioned animals only showed reductions at higher frequencies (~24-45 Hz, high beta/low gamma) and only between GPe and STR. We observed that conditioning of the NPD with the STN signal acted to significantly reduce interactions between STR and GPe in both the forward (STR → GPe, 23-49 Hz, $P<0.001$) and reverse (GPe → STR, 27-49 Hz, $P=0.001$) directions (red bars).

Conditioning the NPD using Local Field Potentials Recorded from GPe

Next, we performed the NPD analysis of recorded signals but this time conditioning the interactions with LFPs recorded from within the GPe (figure 7). We found that the conditioning had the effect of reducing NPD estimates in 6 out of 6 possible connections in the controls and 3 out of 6 in the 6-OHDA-lesioned rats. Most notably we found that the conditioning significantly attenuated (when compared to the unconditioned NPD) the low beta band interaction in the M2 → STR connection for both recordings made in control (red bar, 14-39 Hz, $P<0.001$) and lesioned (blue bar, 14-21 Hz, $P<0.001$) animals implying that signals propagating through STR are highly correlated with that also measured at GPe.

Secondly, we found a reduction of interactions between STR → STN across a wide range of frequencies, again for both control (red bar, 6-49 Hz, $P<0.001$) and lesioned (blue bar, 4-49 Hz, $P<0.001$) recordings suggesting signal routing is strongly mediated by GPe in accordance with the

canonical indirect pathway. Interestingly we found that although beta NPD in the M2 → STN connection was attenuated by conditioning in the control recordings; for the 6-OHDA recordings, the prominent low beta peak in the NPD remained and no significant effect of conditioning was observed. Similarly, the STN → M2 feedback also retained a sharp beta peak that remained significantly increased in recordings corresponding to the 6-OHDA lesion experiments (black bar, 14-20 Hz, P=0.002). Additionally, we found that when conditioning the STR→ M2 NPD estimate with the GPe signal there was an increased strength of interaction in the 6-OHDA treated animals (black bar, 16-21 Hz, P<0.001).

In the high beta/gamma band we found that conditioning with GPe had a large effect in attenuating the NPD in the forward connections (from M2 descending the indirect pathway) in the control animals: M2 → STR (14-39 Hz, P<0.001), M2 → STN (16-49 Hz, P<0.001), and STR → STN (6-49 Hz, P<0.001) (red bars). In the lesion animals only, 2 of the 6 comparisons made with NPD were significantly attenuated in the 20-50 Hz range: STR → STN (4-49 Hz, P<0.001) and STN → STR (31-45 Hz, P=0.004) (blue bars). This would imply that in control animals, high beta/gamma band interactions in both directions between STN and STR are transmitted via (and linearly mixed with) a signal at GPe.

Conditioning the NPD using Local Field Potentials Recorded from the STR

A third set of analyses used the local field potentials recorded at the STR to condition the NPD estimates (figure 8). We found that this had the effect of destroying large parts of the descending interactions (connections from M2 descending the hierarchy of the indirect pathway) in the control animals, namely for M2 → GPe (16-37 Hz, P<0.001) and M2 → STN (16-37 Hz, P<0.001) (red bars). In the lesion recordings, the effect of conditioning split into two ways: 1) Interactions between the STN/GPe were significantly reduced across a very wide band ranging from low-beta to gamma frequencies in both the STN → GPe (8-49 Hz, P<0.001) and GPe → STN (6-49 Hz, P<0.001) coupling (blue bars) and 2) That interactions in the "hyper-direct" M2 → STN connection were not attenuated, although note that the M2 → GPe (likely routed at least in part via the indirect pathway) was suppressed by conditioning with the striatal signal (18-24 Hz, P=0.001, blue bar). This peak is also seen in the feedback connection from STN → M2 where the significant 6-OHDA associated increase in beta feedback reported in previously analysis was found to remain (18-20 Hz, P=0.010, black bar).

Similar to the NPD estimates conditioned with signals recorded at GPe, we found that conditioning with LFPs recorded at STR acted to largely remove the high beta/gamma interactions. In the M2 → GPe connection in control animals we found that high beta/gamma activity was attenuated by STR conditioning (16-37 Hz, P<0.001); furthermore, we observed that 6-OHDA was associated with a significant suppression of activity in this band (27-37 Hz, P<0.001; 41-45 Hz, P=0.004). Additionally, we found that feedback in the high beta/gamma range (for control recordings) from GPe → M2 was significantly attenuated by conditioning with the signal recorded at STR (14-41 Hz, P<0.001, red bar).

Furthermore, this connection from GPe → M2, was significantly strengthened in the 6-OHDA animals (35-41 Hz, P=0.002, black bar).

Conditioning NPD Using Field Potentials Recorded from M2

The final analyses utilized ECoG signals recorded from the M2 to condition the BG NPD estimates (results in figure 9). We found that the NPD estimates conditioned on M2 were generally flattened and lacked distinct peaks at either low beta or high beta/gamma frequencies that were seen typically in the other analyses. Altogether 5 of 6 NPD spectra had no distinct spectral peaks. When testing for significant attenuation of NPD following conditioning we found that only control recordings were significantly attenuated (4 of 6 connections, red bars), with high beta gamma peaks most clearly lost in the STR→ STN and STN → GPe interactions. The loss of features found in the unconditioned NPD (such as beta or gamma peaks) were equivalent for both the control and 6-OHDA recordings.

When testing for the effects of 6-OHDA, we found that the STN → STR connection was significantly altered. We observed a broad peak from 20-40 Hz in the lesion recordings that was not attenuated by M2 conditioning and demonstrated a significant increase in strength associated with dopamine depletion (21-27 Hz, P=0.007, black bar).

Summary of Connectivity Analyses

Using recordings made in control and lesioned rats, we identified functional connectivity between cortical and BG sites that involved either low beta or high beta/gamma oscillations. Broadly speaking, we found that gamma connectivity is sensitive to the conditioning of structures upstream of the STN, particularly GPe and STR, which removes gamma band oscillations from the spectra. In contrast, beta connectivity was found to be robust to partializing using LFPs of any single BG structure. Cortico-subthalamic connectivity in the beta range was unaffected by partialising of GPe or STR, suggesting that M2/STN low beta connectivity is not routed via the indirect pathway. In the next section, we will outline several putative models of oscillatory dynamics and present evidence from our analyses that either support or weaken the plausibility of each model.

Discussion

Hypotheses and evaluation of evidence for signal propagation in the network

We have undertaken a systematic analysis of a dataset involving multisite ECoG/LFP recordings of the cortico-basal ganglia circuit that contains data from a set of dopamine-intact control rats and another set of rats with chronic dopamine depletion induced by a unilateral injection of 6-OHDA. We will next discuss evidence for competing theories of the propagation of oscillatory activity across the Parkinsonian cortico-basal ganglia circuit. We emphasise that our results are indicative of the transmission of rhythmic activity in the circuit and cannot directly access the mechanisms that generate these rhythms. However, as we will argue, results describing the patterns of synchronized activity across

the network and the changes that occur to them following dopamine depletion proffer an important insight into how pathological rhythms differentially engage functional networks.

Mechanisms of the Flow of Beta Rhythms in the Basal Ganglia Circuit

Here we will evaluate the evidence provided by the analyses reported here in light of a number of proposed theories concerning the generation and propagation of beta-band activity in the network and the changes that occur during dopamine depletion that lead to its amplification. This work is summarised in table 1.

Hypothesis 1: Dopamine depletion in the basal ganglia induces increased beta resonance in the cortical/STN "long-loop".

Previous authors have suggested that pathological beta rhythms are generated from the strengthening of a long cortical feedback loop that returns from basal ganglia output nuclei via the thalamus. Strengthened coupling is proposed to facilitate pathological resonance at beta frequencies (Brown 2007; van Albada and Robinson 2009; Dovzhenok and Rubchinsky 2012; Pavlides et al. 2015). The first step towards verifying the plausibility of this hypothesis involves determining whether there is indeed functional connectivity between STN and M2 in the beta band, and whether this occurs independently of the cortico-striatal inputs to the indirect pathway.

Analysis of the iCOH for the M2/STN pairing suggests that functional connectivity in the beta band is significantly strengthened in the lesioned animals compared to controls (figure 4). Analysis with NPD demonstrates that there is a beta peak in the directed coherence in the low beta range in the forward M2 → STN connection for both the control and 6-OHDA animals. Furthermore, in the lesioned animals, the feedback connection (STN → M2) is significantly strengthened over that measured in the controls. Neither the hyper-direct M2 → STN connection, nor the subthalamo-cortical feedback (STN → M2) is diminished by either conditioning with signals from the GPe or STR in the lesioned animals (figure 7 and figure 8). This suggests a reciprocal pathway between STN and M2 that is routed independently of STR or GPe, most likely feeding back directly via the BG output nuclei. In contrast, in control rats, NPD of the feedback connections at beta frequencies are significantly decreased by conditioning with the STR signal in the forward (M2 → STN), and backward (STN → M2) directions, suggesting that in the dopamine-intact anaesthetised state, beta band activity is routed via STR, whilst the hyper-direct pathway is relatively quiescent. These findings support the idea that the dopamine-depleted state is associated with a strengthening of the hyper-direct pathway and subthalamo-cortical feedbacks.

Notably, this pathway is not active in isolation but coexists with beta propagation occurring along striatal indirect pathway projections. Most notably, it was found that conditioning of the NPD with LFPs recorded from the STN (figure 6) does not act to remove the 6-OHDA lesion associated beta NPD in the structures 'upstream' of the STN (i.e. the STR and GPe). NPD in the low beta range is significant in both directions along parts of the network involving either M2, STR or GPe. We find that striatal-

subthalamic interactions are strongly modulated by the GPe signal, a finding in line with propagation down the canonical indirect pathway. Future work to validate the long-loop hypothesis would involve the conditioning of the STN → M2 NPD using signals recorded from BG output nuclei (either internal globus pallidus (GPi /EPN in rat) and/or SNr) or their major targets in the thalamus. If these signals were available, then it would be possible better determine the routing of the cortical return of BG beta activity from the STN.

Hypothesis 2: Pathological beta is generated from strengthening of the reciprocally coupled STN/GPe circuit.

A separate hypothesis concerning the generation of pathological beta rhythms in the basal ganglia considers the reciprocally coupled STN/GPe circuit from which increased coupling associated with the loss of dopamine induces a pathological beta resonance that spreads across the rest of the network (Plenz and Kital 1999; Bevan et al. 2002; Holgado et al. 2010; Tachibana et al. 2011).

We note that conditioning the NPD with the M2 signal does not remove the strong STN → GPe directed connectivity, but it does attenuate the GPe → STN (figure 9). This indicates that activity feeding back onto GPe from STN has a sufficiently unique temporal content so as not be partialized out by the cortical ECoG, suggesting that pathological beta activity could be generated by some resonance phenomenon arising from the tight, reciprocal coupling of STN and GPe. However, a number of the analyses presented here suggest that pathological beta does not originate from an autonomous STN/GPe resonator. These can be summarised as follows: 1) Comparison of forward and backward NPD for STN/GPe interactions shows strong asymmetry, with the GPe→ STN connection predominating; 2) conditioning of the NPD using the LFPs recorded at the STR significantly reduces the strength of both GPe → STN and STN → GPe NPDs in a way that appears to be irrespective to dopaminergic state (figure 8), suggesting that beta activity in these structures results from beta oscillations propagating through striatum; 3) conditioning the NPD with LFPs recorded at the STN (figure 6) does not act to remove the upstream 6-OHDA associated beta NPD between STR or GPe (although it does significantly weaken beta NPD in the control animals); 4) GPe conditioned NPD analysis does not impair pathological M2/STN beta interactions (figure 7), suggesting that the beta found at STN can be, at least in part, generated independently of a signal found at GPe. The evidence given in point (1) may arise from the very tight coupling of the STN/GPe pair, if full phase synchronization is occurring then the phase alignment between the two nuclei may mislead the NPD to determine the phase leading population to be the drive, when in actuality there is strong reciprocal coupling. The evidence in (2) and (3) points towards a mechanism of striatal modulation of the STN/GPe circuit, perhaps via a pallidal-striatal feedback mechanism such as that described by (Corbit et al. 2016). Taken together we argue these findings provide evidence against pathological beta synchronization in the network arising from dissemination of an autonomously generated rhythm in a STN/GPe “resonator”.

Hypothesis 3: Beta arises through aberrant striatal activity and facilitation of downstream hyper-synchrony.

It has been proposed that aberrant striatal activity is involved in the emergence of pathological beta rhythms in the BG arises due to changes to local dynamics within striatum (McCarthy et al. 2011; Damodaran et al. 2015; Sharott et al. 2017); and/or a modification of striatal influence on the STN/GPe sub-circuit (Terman et al. 2002; Kumar et al. 2011b; Sharott et al. 2017). From iCOH analysis of signals recorded within striatum we do not find any local non-zero phase interactions (unlike that which we find at STN). This finding would suggest that striatal-striatal transmission is sparse, or phase aligned. Our results show that NPD measured at both the STN and GPe are significantly weakened by conditioning with STR signals (figure 8) implying that striatal beta band activity propagates down the indirect pathway. This would be in the line with the recent demonstration that the firing of indirect pathway spiny projection neurons is aberrantly (and selectively) entrained to exaggerated beta oscillations in lesioned rats (Sharott et al. 2017).

The weakening of NPD interactions from STR → GPe and GPe→ STN when conditioning with M2 ECoG (figure 9), and only for the dopamine intact controls, may suggest that dopamine depletion results in increased autonomy of the striatal (and indirect pathway) beta rhythm from beta at M2. In support of this hypothesis, we also demonstrate that conditioning of the STR → GPe NPD with the STN signal is only effective (within the low beta range) in the control condition. This again demonstrates that 6-OHDA lesioning results in a striatal signal that retains information independent from that found at STN, providing evidence that it is likely the change of striatal output that occurs following dopamine depletion. There is however some ambiguity as to whether the separation of the striatal signal from that at the STN occurs due to changes to striatal dynamics or instead a change of direct input to the STN such as from a strengthened hyperdirect input as discussed in hypothesis 1.

Hypotheses of the Origins/Routing of High Beta/Gamma Oscillations

The presence of high beta/gamma oscillations in the subcortical network has been noted by a number of authors (Brown et al. 2002; Humphries et al. 2006; Berke 2009; Sharott et al. 2009; van der Meer et al. 2010; Nicolás et al. 2011) but our understanding of the functional propagation of high beta/gamma oscillations through the network is limited. An evaluation of the evidence we present in this paper is summarised in table 2. We report gamma activity in the LFPs as well as connectivity in the range 30-60 Hz which is in good agreement with that previously reported in anaesthetised rats (Magill et al. 2004; Sharott et al. 2005b, 2009). Gamma activity in the awake and moving rat has also been reported, albeit at slightly higher frequencies (Brown et al. 2002; Brazhnik et al. 2012; Delaville et al. 2014).

Hypothesis 4: High beta/gamma enters the subcortical network via the hyper-direct M2 → STN connection.

Results from analyses which used iCOH to investigate non-zero lag correlations between BG structures and the cortex suggested that gamma interactions are routed in a way that bypasses STR as a gamma peak is absent in the M2 ↔ STR connection (figure 4). This effect is most clear in the control recordings but also to a lesser extent in the 6-OHDA experiments. The hyper-direct pathway is the other principal source of cortical input to the BG, therefore the marked weakness of gamma interaction in the M2/STR when compared to the M2/STN iCOH spectra may imply that the hyper-direct pathway is responsible for gamma input to the network.

However, whilst there is a large peak in the high-beta/low-gamma band NPD for the M2 → STN interaction (figure 5), if we examine the same connection but conditioned on LFPs either recorded at STR (figure 7) or GPe (figure 8) we see that the conditioning significantly reduces NPD in the control animals (M2 → STN conditioned on STR and M2 → STN conditioned on GPe), suggesting any directed coherence between M2 and STN in these animals is routed via striatal-pallidal connections. Furthermore, if we condition the NPD with LFPs recorded at the STN (figure 6), we see that gamma interactions remain in the upstream components (M2 → STR, M2 → GPe) again suggesting striatal-pallidal connectivity is vital in the propagation of gamma rhythms. When taken together, these data do not supply strong evidence that the source of high beta/gamma input in the network is transferred by a hyper-direct cortico-subthalamic route.

Hypothesis 5: Gamma enters the network via cortico-striatal inputs and reaches STN via the indirect pathway in a dopamine dependent manner.

An alternative to high beta/gamma oscillations entering via hyper-direct STN input is that they are channelled via the cortico-striatal indirect pathway. The clearest results of the NPD analysis in the high beta/gamma band can be seen to be for the forward NPDs originating from M2 and passing on to the subcortical regions (figure 5). Connections M2 → STR, M2 → GPe, and M2 → STN all show high values of NPD in this frequency band (> 0.15) suggesting that most of the gamma is directed from the cortex. Furthermore, conditioning the NPD with either LFPs recorded at the STR (figure 8) or GPe LFPs (figure 7) acts to remove gamma interactions both upstream and downstream of the STR (with respect to the indirect pathway). Subsequently, conditioning of the NPD with STN (figure 6) is less effective at attenuating gamma band interactions than when using signals higher in the indirect pathway, suggesting that the gamma descends the hierarchy, from either a cortical or striatal source. Notably, we observed that STN conditioned NPD did not act to attenuate feedback connections from GPe or STR back to the M2. This would suggest routing of gamma to the M2 in a way that occurs independently of STN.

In attempt to elucidate the source of the gamma activity we conditioned the NPD on the cortical ECoG (figure 9). We find that gamma connectivity in the control recordings and in dopamine depletion states acts to significantly reduce NPD coefficients for the GPe → STN and STR → STN connections, yet the feedback connection STN → STR is unaffected. This connection in the control animals shows a peak from 18-42 Hz which is significantly larger than in the lesioned animals. This is in agreement with the hypothesis that gamma rhythms are pro-kinetic; this idea is also supported by patients' data (Sharott et al. 2014). Furthermore, these findings suggest that gamma activity is directed to upstream components of the indirect pathway in a way independent of M2, perhaps mediated via a subcortical feedback loop.

Hypothesis 6: High beta/gamma is generated locally within the basal ganglia network either at STR, STN or GPe

The finding that conditioning the NPD with cortical ECoG does not entirely abolish gamma connectivity within the BG suggests a possible subcortical high beta/gamma generator, or alternatively a source in the cortex that has not been measured in our experiments. Work by Kondabolu et al. (2016) has demonstrated that the optogenetic activation of striatal cholinergic interneurons is sufficient to generate gamma rhythms locally, although not in a way clearly separable from low frequency beta. However, when applying iCOH to signals recorded within STR we find no evidence for local interactions in the high beta/gamma band. Simulations of the BG spiking network by Humphries et al. (2006) suggest that upper-gamma band (40-80 Hz) activity can arise as a result of coupling between the STN and GPe. When we conditioned the NPD with LFPs recorded from either the GPe (figure 7) or STR (figure 8), we found that interactions in the high beta/gamma frequency ranges were abolished in the majority of other subcortical interactions. This would imply that these GPe and STR structures are necessary for the propagation of high beta/gamma interactions in the both the control and 6-OHDA lesion animals. This in combination with the evidence provided for hypothesis 5 suggests that high beta/gamma can originate at either STR or GPe and then propagate to downstream structures. Backward gamma interactions from GPe to STR are apparent in the NPD conditioned on either M2 or STN, suggesting the STR signal is the result of local propagation of a gamma signal from GPe. From the canonical circuit perspective it is not clear how gamma passes upstream from GPe. However, a substantial proportion of GPe neurons that innervate the striatum have been shown to exist, with one GPe cell type (arkypallidal neurons) projecting exclusively to striatum (Mallet et al. 2012; Abdi et al. 2015; Hegeman et al. 2016). This same pathway has been proposed by Corbit et al. (2016) to promote synchronization in the low beta range but the same arguments are likely to apply to high beta/low gamma frequencies.

Summary of Findings

In this paper, we have investigated the propagation of oscillatory activity through connected regions of the cortico-basal ganglia network. We have applied a novel model-free method of partialized directed

connectivity to achieve a systematic deconstruction of the propagation of rhythmic activity between regions of the network inferred from the LFPs and ECoGs recorded at multiple sites within that network. Using the 6-OHDA-lesioned rat model of Parkinsonism, we demonstrate marked differences in the patterns functional connectivity that result as a consequence of dopamine depletion in the BG.

We find widespread beta synchronization of LFPs across the network that is strongly associated with chronic dopamine depletion. With regards to functional beta connectivity in the network we find evidence for:

1. An increased cortical drive to the basal ganglia following dopamine depletion.
2. Significant beta-band connectivity between structures interacting with the STN that is independent of activity upstream in the indirect pathway (at STR and GPe). This is likely to originate from the 'hyperdirect' cortico-subthalamic input.
3. Increase in feedback of BG structures to M2 after dopamine depletion, proffering evidence in favour of a hypothesis of dopamine-dependent modulation of the long re-entrant cortico-BG-thalamo-cortical loop.
4. Activity dynamics of the STN/GPe sub circuit that are partly dependent upon drive from striatum.
5. A feedback from STN to STR that is independent of M2 and significantly strengthened after dopamine depletion, suggesting a strengthening of recurrent subcortical circuits.

Furthermore, we provide evidence for the existence of high beta/gamma synchrony within the network, with evidence that dopamine depletion acts to weaken these rhythms. We summarise our findings with respect to high beta/gamma band interactions in the following:

1. Gamma propagates down the indirect pathway from STR to GPe to STN. This activity is likely to be generated at the level of the cerebral cortex.
2. Evidence of gamma activity found at STN that is independent of M2 and evidence for a subcortical return of subthalamic outputs back to striatum.
3. Evidence for gamma activity returning to the cortex that is independent of STN, perhaps indicating propagation through the direct pathway.

Propagation of Low Beta via two Coexisting but Distinct Streams

In the case of low beta oscillations, we find our data most strongly support a hypothesis that in the dopamine-depleted condition, beta propagation in the network is biased to favour low beta synchrony via induction of a long cortico-subthalamic loop that inputs to the BG via the hyper-direct pathway. Furthermore, we see evidence that the return connection from STN to M2 is significantly stronger in the lesioned animals when compared to dopamine-intact controls. This provides supporting evidence for the notion that pathological beta amplification arises from entrainment of the re-entrant cortical/STN

loop (Brittain and Brown 2014). We speculate that strengthening of the hyper-direct input acts to "short-circuit" the network, such that transmission of information along the indirect pathway is compromised. Oswal et al. (2016) have provided evidence that deep brain stimulation in patients acts to selectively suppress activity mediated synchrony between mesial premotor regions and the STN which is proposed to be mediated by the hyper-direct pathway. In the "hold your horses" model of the STN's role in decision making (Frank 2006; Frank et al. 2007), the hyper-direct pathway is proposed to provide a cortical veto signal which may act to suppress premature action. In the case of PD, over activity of this circuit via increased resonance may act to lock the network into a state that ultimately supresses action and movement. These findings are in agreement with previous research which have found good evidence for bidirectional connectivity between STN and cortex (Lalo et al. 2008; Jávor-Duray et al. 2015).

This hypothesis requires further testing through analysis of the role of the BG output nuclei at GPi or SNr (or their targets in the thalamus) in the propagation of activity. This could be achieved using a functional 'lesion' approach like that described in this paper. Furthermore, biophysical modelling of the cortico-subthalamic loop may yield insight as to whether this is a plausible mechanism given the known conduction delays for the connections in the network. Long feedback loops involving cortex have been demonstrated to be capable of generating oscillatory activity (Leblois et al. 2006; Pavlides et al. 2015). Work by Shouno et al. (2017) suggests that the required delay for the return of the beta oscillation from STN to cortex may be too great to support resonance in the low beta band and possibly the engagement of shorter subcortical loops either subcortical-thalamic loops (McHaffie et al. 2005) or activity of recurrent subthalamo-striatal projections (Sato et al. 2000; Koshimizu et al. 2013) may be more suitable candidates for supporting beta oscillations through resonance.

The analysis presented here also suggests that a cortico-subthalamic pathway is not the exclusive pathway for beta rhythms within the network, yet may be necessary for enhancement of the STN feedback to cortex that may induce pathological resonance. We would suggest that both the hyperdirect and indirect routes for beta propagation coexist. These two pathways could originate from and be driven by, distinct populations of cortical projections neurons (namely those of the pyramidal tract and intra-telencephalic projections, respectively) and so are likely to show a degree of independence from one another. The data presented here also suggest a second pathway upstream of STN involving the STR that is most evident in the recordings from control rats. We suggest that both pathways contain signals shared by activity measured in the cortical ECoG: conditioning of the NPD acts to remove beta peaks from the majority of connections that were analysed, leaving just beta coherence at the STR → STN connection. These findings support the hypothesis that dopamine cell loss acts to increase the sensitivity of the STR to cortical inflow, disrupting the striatum's role in gating activity to the remainder of the circuit (Magill et al. 2001; Tseng et al. 2001; Sharott et al. 2017).

Notably, our data do not support the hypothesis of beta generation via an autonomous STN/GPe pacemaker network, as directional coherence between the two is heavily attenuated by conditioning with LFPs recorded upstream in the STR and there is significant asymmetry in the NPD with the globus pallidus drive predominating. In agreement, Moran et al. (2011) found evidence for a weakening of the STN to GPe feedback connection in the dopamine depleted state, conflicting with the STN/GPe resonance hypothesis. It may be the case that tight coupling of the STN and GPe results in a near fixed phase relationship in which there is reciprocal coupling yet from the perspective of phase, the GPe appears to lead.

Estimates of effective connectivity from DCM studies have also suggested that input from cortex to STN is strengthened in the Parkinsonian state (Moran et al. 2011), a finding consistent with the idea that dopamine enforces cortical influence upon the STN/GPe network (Magill et al. 2001; Leblois 2006; Leblois et al. 2006; Holgado et al. 2010). It is possible that in PD, cortical activity subsumes the STR as the primary driver of the STN/GPe sub-circuit, effectively acting to "short-circuit" the system. It has been demonstrated that movement is associated with a decreased cortico-pallidal coherence during movement in humans (van Wijk et al. 2017) suggesting that disengagement of cortical influence via this pathway is pro-kinetic. Thus pathological resonance may arise following dopamine depletion through a compensatory mechanism of increased hyperdirect input following an altered or reduced striatal output (Kumar et al. 2011a; Damodaran et al. 2015). In the healthy system it has been proposed that this works to actively de-correlate spiking activity between the two structures (Wilson 2013). The action of dopamine upon these inputs is likely to lead to the promotion of beta amplifying phase alignments between STN and GPe such as that observed by Cagnan, Duff, & Brown (2015).

Dopamine Depletion is Associated with an Increased Subthalamo-Striatal Feedback

Taken together, the analyses presented here speak to the existence of a high beta/low gamma rhythm that is in general reduced by dopamine depletion. Specifically, our results indicate that connectivity in the frequency band 27-34 Hz is attenuated by the 6-OHDA lesion. Experiments investigating LFPs in the motor cortex of moving rats have demonstrated an increase in activity in this band during movement suggesting that activity at these frequencies in M2 and SNr is pro-kinetic (Brazhnik et al. 2012). Our data would suggest that high beta/gamma activity in the normal network is predominantly driven by the cortex as evidenced by: 1) the unconditioned NPD indicates that gamma is prominently in the forward direction leading from cortex to subcortical sources; and 2) conditioning the NPD on ECoG recorded at M2 acts to diminish the subcortical directional coherence across a wide band for all connections not involving STN. However, evidence by Zold and colleagues has demonstrated that oscillatory activity >20 Hz in corticostriatal afferents is not effectively transmitted through the striatum (Zold et al. 2012) suggesting that the actual mechanism is likely to be more complicated.

Furthermore, following partialization some interactions involving STN do remain. In particular we provide evidence for a significant strengthening of feedback from STN to STR in the lesioned animals in the high beta/gamma band. We speculate that this signal is facilitated through the strengthening of subcortical loops such as that of the thalamo-striatal pathways (McHaffie et al. 2005). Thalamic afferents make up to at least 25% of input onto spiny projection neurons in the STR (Doig et al. 2010; Smith et al. 2014) but have been far less studied than cortical inputs. Work investigating synaptic remodelling following 6-OHDA depletion in mice has suggested that thalamo-striatal inputs to medium spiny neurons are shifted in favour of the indirect pathway (Parker et al. 2016) perhaps enhancing striatal return of subthalamic activity in a mechanism independent of cortex.

Segregation of Low Beta and High Beta/Gamma Functional Networks

Our analyses present a clear separation in the patterns of inter-areal synchronization between low beta and high beta/low gamma frequencies. We find pathological low beta correlations to be present across large parts of the network, and resistant to conditioning with signals from connected structures. In contrast, high beta/gamma shows a much more hierarchical organization, descending the indirect pathway and possibly looping back subcortically through subthalamic-striatal feedback. Furthermore, high beta/gamma correlations appear to be weakened by the 6-OHDA lesion.

Multiple studies investigating the electrophysiology of patients with PD (Priori et al. 2004; López-Azcárate et al. 2010) have found evidence for the functional differentiation between low and high beta frequency activity. Low beta is found to be increased by dopamine depletion and correlates with bradykinetic/rigid symptoms in patients, whereas high beta is less responsive to dopamine changes. Interestingly, dopamine replacement in patients has been shown to decouple high and low beta frequencies when analysing with spectral bicoherence (Marceglia et al. 2006). Cortico-subthalamic coherence is also found at this frequency in patients, although again this is largely unresponsive to dopamine (Litvak et al. 2011b). We also find evidence for high beta coherence between BG and cortex although unlike that found in patients, we find this connectivity to be weakened and shifted to low beta frequencies by 6-OHDA induced dopamine depletion.

Study Limitations

Incomplete Signals for Conditioning

The use of partial coherence for inferring neural connectivity is not in itself a novel approach (Rosenberg et al. 1998; Eichler et al. 2003; Salvador et al. 2005; Medkour et al. 2009), and the application of the partialized NPD to LFPs recorded in the rat hippocampus has been previously reported (Halliday et al. 2016). However, these analyses assume that the signals used for conditioning completely capture the activity going through the proposed pathway. This however is unlikely to be entirely the case due to the finite sampling of the structures afforded from the use of electrodes. That said the large number of channels used for recordings in the present study ensure that multiple samples

are obtained from within each brain structure. In the data presented here, subcortical structures were recorded from between 2-8 different channels which were all used to condition the estimate of directed coherence. It should also be noted that this sampling limitation is likely to apply most to the larger structures that were analysed, namely the motor cortex and striatum, whereas recordings from the smaller sized STN are more likely to capture a larger share of the total activity. This factor must be considered when interpreting conditioning of the NPD with respect to STR signals. It could be the case that M2 → STN connectivity remains in the face of conditioning with the STR LFP as a result of incomplete sampling of neural fields within striatum.

Inference of Connectivity from Non-Spiking Brain Activity

This study is based upon an analysis of mesoscale recordings of brain activity as measured either in the ECoG or the LFP. Transmission of information in the brain is due to axonal propagation of action potentials is not explicitly captured in these signals. LFPs and ECoG comprise a conglomerate of sub- and supra- threshold events that may or may not be tied to spike activity and so direct inference of neurophysiological connectivity *per se* is limited by this. Nonetheless, spike timing has been shown to tightly correlate with negative deflection of the LFP (Destexhe et al. 1999) and increasing evidence that the field itself modulates neural activity is emerging (Qiu et al. 2015; Goldwyn and Rinzel 2016). With respect to the basal ganglia, it has been previously demonstrated by Mallet and colleagues that beta-band activity in the LFPs recorded at STN and GPe of lesioned rats are associated with increased bet-frequency synchronization of action potential firing by neurons in these structures (Mallet et al. 2008a, 2008b) but see also Magill et al. (2004) where coupling of GPe units and slow wave activity in the LFP is relatively weak in dopamine-intact rats. Furthermore, we provide evidence for the existence of temporally lagged correlations between rhythmic local field potentials recorded between distinct regions of the cortico-BG network that imply causation from one signal to another, a phenomenon that would itself not be possible without the transmission of action potentials. Future work will require an investigation to determine whether directional interactions are ascertainable from multiunit activity and how this relates to lagged synchronization of LFPs.

Limits to Inference of Causal Interactions and Mechanisms from Neurophysiological Signals Alone

In this paper, we aim to infer how neural activity propagates across the BG network by investigating the statistical relationships between brain signals. The challenges that this approach face are well documented (Friston 2011; Bastos and Schoffelen 2016). With respect to this study, the benefits that that we claim for using a model free, non-parametric approach (namely agnosticism to the underlying generating mechanisms of the data) may in turn limit the degree of inference that can be made. Estimates of directed functional connectivity in this paper follow from the assumptions that temporal precedence is indicative of causation. It is however well documented that zero lag synchronization can emerge from neural circuits with particular (but not unusual) network motifs (Vicente et al. 2008; Viriyopase et al.

2012; Gollo et al. 2014). Additionally, "anticipatory" synchronization in which positive lags arise from a directed input have also been described in theoretical neural dynamics (Ambika and Amritkar 2009; Ghosh and Roy Chowdhury 2010; Matias et al. 2011). The anatomically tightly coupled STN-GPe sub-circuit is a prime candidate for which these phenomena may permit vanishingly small phase lags that make the interactions blind to NPD. Answers to these problems may be given in the future by the fitting of biophysical models to the data presented in this paper. This would provide a well-defined, quantitative description of the potential mechanisms that act to generate the phenomena we have described.

Moreover, we must stress that analysis of functional connectivity cannot access directly the mechanisms that generate sustained neural oscillations and their synchronization. This requires direct experimental manipulations of connections in the network such as that by Tachibana et al. (2011). Nonetheless, the patterns of propagation in functional networks and the changes that occur to them following a manipulation such as the 6-OHDA ablation of dopamine neurons leave behind a signature that is accessible to the tools of functional connectivity. Further, the ability to apply systematic "functional lesions" such as that afforded by the conditioned NPD analysis, only acts to more increase our ability to infer the generative mechanisms of the observed data.

Conclusion

Overall, we provide a systematic deconstruction of the propagation of pathological rhythms across the Parkinsonian cortico-basal ganglia circuit *in vivo*. These findings strengthen our understanding of how normal and pathological rhythms propagate across the network. Our work highlights the importance of considering non-canonical connections in the network, in particular the activity of recurrent subcortical projections that may act to amplify pathological activity within the BG. Future work will aim to understand the exact changes to the network required to generate the patterns of functional connectivity presented here, as well as to investigate the relationship with spiking activity in the network.

Acknowledgments

We thank Dr N. Mallet for acquiring some of the primary data sets. T.O.W. thanks UCL CoMPLEX for their continued funding and support.

Funding

Medical Research Council UK (awards UU138197109, MC_UU_12020/5 and MC_UU_12024/2 to P.J.M.; MC_UU_21024/1 to A.S.). Parkinson's UK (Grant G-0806 to P.J.M.). S.F.F. receives funding from UCLH BRC. Engineering Research Council UK (awards EPSRC EP/F500351/1 to T.O.W.; EP/N007050/1 to D.H.). The Wellcome Trust Centre for Neuroimaging is funded by core funding from the Wellcome Trust (539208).

References

Abdi A, **Mallet N**, **Mohamed FY**, **Sharott A**, **Dodson PD**, **Nakamura KC**, **Suri S**, **Avery S V**, **Larvin JT**, **Garas FN**, **Garas SN**, **Vinciati F**, **Morin S**, **Bezard E**, **Baufreton J**, **Magill PJ**. Prototypic and arkypallidal neurons in the dopamine-intact external globus pallidus. *J Neurosci* 35: 6667–88, 2015.

van Albada SJ, **Robinson PA**. Mean-field modeling of the basal ganglia-thalamocortical system. I: Firing rates in healthy and parkinsonian states. *J Theor Biol* 257: 642–663, 2009.

Ambika G, **Amritkar RE**. Anticipatory synchronization with variable time delay and reset. *Phys Rev E* 79: 56206, 2009.

Bastos AM, **Schoffelen J-M**. A Tutorial Review of Functional Connectivity Analysis Methods and Their Interpretational Pitfalls. *Front Syst Neurosci* 9: 175, 2016.

Berke JD. Fast oscillations in cortical-striatal networks switch frequency following rewarding events and stimulant drugs. *Eur J Neurosci* 30: 848–859, 2009.

Beudel M, **Oswal A**, **Jha A**, **Foltynie T**, **Zrinzo L**, **Hariz M**, **Limousin P**, **Litvak V**. Oscillatory Beta Power Correlates With Akinesia-Rigidity in the Parkinsonian Subthalamic Nucleus. *Mov Disord* 32: 174–175, 2017.

Bevan MD, **Magill PJ**, **Terman D**, **Bolam JP**, **Wilson CJ**. Move to the rhythm: oscillations in the subthalamic nucleus–external globus pallidus network. *Trends Neurosci* 25: 525–531, 2002.

Bolam JP, **Hanley JJ**, **Booth PA**, **Bevan MD**. Synaptic organisation of the basal ganglia. *J Anat* : 527–42, 2000.

Brazhnik E, **Cruz A V.**, **Avila I**, **Wahba MI**, **Novikov N**, **Ilieva NM**, **McCoy AJ**, **Gerber C**, **Walters JR**. State-Dependent Spike and Local Field Synchronization between Motor Cortex and Substantia Nigra in Hemiparkinsonian Rats [Online]. *J Neurosci* 32, 2012. http://www.jneurosci.org/content/32/23/7869.long [2 May 2017].

Bressler SL, **Menon V**. Large-scale brain networks in cognition: emerging methods and principles. *Trends Cogn Sci* 14: 277–290, 2010.

Brittain J-S, **Brown P**. Oscillations and the basal ganglia: motor control and beyond. *Neuroimage* 85: 637–647, 2014.

Brown P. Abnormal oscillatory synchronisation in the motor system leads to impaired movement. *Curr Opin Neurobiol* 17: 656–664, 2007.

Brown P, **Kupsch A**, **Magill PJ**, **Sharott A**, **Harnack D**, **Meissner W**. Oscillatory Local Field

Potentials Recorded from the Subthalamic Nucleus of the Alert Rat. 2002.

Brown P, **Oliviero A**, **Mazzone P**, **Insola A**, **Tonali P**, **Di Lazzaro V**. Dopamine Dependency of Oscillations between Subthalamic Nucleus and Pallidum in Parkinson's Disease [Online]. *J Neurosci* 21: 1033–1038, 2001. http://www.jneurosci.org/content/21/3/1033.abstract [4 Jan. 2016].

Cagnan H, **Duff EP**, **Brown P**. The relative phases of basal ganglia activities dynamically shape effective connectivity in Parkinson's disease. *Brain* 138: 1667–1678, 2015.

Corbit VL, **Whalen TC**, **Zitelli KT**, **Crilly SY**, **Rubin JE**, **Gittis AH**. Pallidostriatal Projections Promote β Oscillations in a Dopamine-Depleted Biophysical Network Model. *J Neurosci* 36: 5556–71, 2016.

Damodaran S, **Cressman JR**, **Jedrzejewski-Szmek Z**, **Blackwell KT**. Desynchronization of Fast-Spiking Interneurons Reduces β-Band Oscillations and Imbalance in Firing in the Dopamine-Depleted Striatum [Online]. *J Neurosci* 35, 2015. http://www.jneurosci.org/content/35/3/1149.long [19 Jul. 2017].

Deco G, **Jirsa VK**, **Robinson PA**, **Breakspear M**, **Friston K**. The dynamic brain: from spiking neurons to neural masses and cortical fields. *PLoS Comput Biol* 4: e1000092, 2008.

Deco G, **Senden M**, **Jirsa V**. How anatomy shapes dynamics: a semi-analytical study of the brain at rest by a simple spin model. *Front Comput Neurosci* 6: 68, 2012.

Delaville C, **Cruz A V**, **McCoy AJ**, **Brazhnik E**, **Avila I**, **Novikov N**, **Walters JR**. Oscillatory Activity in Basal Ganglia and Motor Cortex in an Awake Behaving Rodent Model of Parkinson's Disease. *Basal Ganglia* 3: 221–227, 2014.

DeLong M, **Wichmann T**. Changing views of basal ganglia circuits and circuit disorders. *Clin EEG Neurosci* 41: 61–7, 2010.

Destexhe A, **Contreras D**, **Steriade M**. Spatiotemporal Analysis of Local Field Potentials and Unit Discharges in Cat Cerebral Cortex during Natural Wake and Sleep States [Online]. *J Neurosci* 19: 4595 LP-4608, 1999. http://www.jneurosci.org/content/19/11/4595.abstract.

Doig NM, **Moss J**, **Bolam JP**. Cortical and Thalamic Innervation of Direct and Indirect Pathway Medium-Sized Spiny Neurons in Mouse Striatum [Online]. *J Neurosci* 30, 2010. http://www.jneurosci.org.libproxy.ucl.ac.uk/content/30/44/14610 [24 Aug. 2017].

Donoghue JP, **Wise SP**. The motor cortex of the rat: Cytoarchitecture and microstimulation mapping. *J Comp Neurol* 212: 76–88, 1982.

Dostrovsky J, **Bergman H**. Oscillatory activity in the basal ganglia--relationship to normal physiology and pathophysiology. *Brain* 127: 721–722, 2004.

951 **Dovzhenok A**, **Rubchinsky LL**. On the Origin of Tremor in Parkinson's Disease. *PLoS One* 7, 2012.

952 **Eichler M**, **Dahlhaus R**, **Sandkuhler J**. Partial correlation analysis for the identification of synaptic
953 connections. *Biol Cybern* 89: 289–302, 2003.

954 **Eusebio a**, **Thevathasan W**, **Doyle Gaynor L**, **Pogosyan a**, **Bye E**, **Foltynie T**, **Zrinzo L**, **Ashkan**
955 **K**, **Aziz T**, **Brown P**. Deep brain stimulation can suppress pathological synchronisation in
956 parkinsonian patients. *J Neurol Neurosurg Psychiatry* 82: 569–573, 2011.

957 **Frank MJ**. Hold your horses: A dynamic computational role for the subthalamic nucleus in decision
958 making. *Neural Networks* 19: 1120–1136, 2006.

959 **Frank MJ**, **Samanta J**, **Moustafa AA**, **Sherman SJ**. Hold your horses: impulsivity, deep brain
960 stimulation, and medication in parkinsonism. *Science* 318: 1309–12, 2007.

961 **Fries P**. A mechanism for cognitive dynamics: neuronal communication through neuronal coherence.
962 *Trends Cogn Sci* 9: 474–480, 2005.

963 **Fries P**. Rhythms for Cognition: Communication through Coherence. *Neuron* 88: 220–235, 2015.

964 **Friston KJ**. Functional and Effective Connectivity: A Review. *Brain Connect* 1: 13–36, 2011.

965 **Ghosh D**, **Roy Chowdhury A**. Lag and anticipatory synchronization based parameter estimation
966 scheme in modulated time-delayed systems. *Nonlinear Anal Real World Appl* 11: 3059–3065, 2010.

967 **Gillies A**, **Willshaw D**. Models of the subthalamic nucleus: The importance of intranuclear
968 connectivity. *Med Eng Phys* 26: 723–732, 2004.

969 **Goldwyn JH**, **Rinzel J**. Neuronal coupling by endogenous electric fields: cable theory and
970 applications to coincidence detector neurons in the auditory brain stem. *J Neurophysiol* 115: 2033–51,
971 2016.

972 **Gollo LL**, **Mirasso C**, **Sporns O**, **Breakspear M**. Mechanisms of Zero-Lag Synchronization in
973 Cortical Motifs. *PLoS Comput Biol* 10: e1003548, 2014.

974 **Halliday D**, **Rosenberg JR**, **Amjad A**, **Breeze P**, **Conway BA**, **Farmer SF**. A framework for the
975 analysis of mixed time series/point process data—Theory and application to the study of physiological
976 tremor, single motor unit discharges and electromyograms. *Prog Biophys Mol Biol* 64: 237–278,
977 1995.

978 **Halliday DM**, **Senik MH**, **Stevenson CW**, **Mason R**. Non-parametric directionality analysis –
979 Extension for removal of a single common predictor and application to time series. *J Neurosci*
980 *Methods* 268: 87–97, 2016.

981 **Hammond C**, **Bergman H**, **Brown P**. Pathological synchronization in Parkinson's disease: networks,

models and treatments. *Trends Neurosci* 30: 357–364, 2007.

Hanslmayr S, **Staudigl T**, **Fellner M-C**. Oscillatory power decreases and long-term memory: the information via desynchronization hypothesis. *Front Hum Neurosci* 6: 74, 2012.

Hegeman DJ, **Hong ES**, **Hernández VM**, **Chan CS**. The external globus pallidus: progress and perspectives. *Eur J Neurosci* 43: 1239–1265, 2016.

Holgado AJN, **Terry JR**, **Bogacz R**. Conditions for the Generation of Beta Oscillations in the Subthalamic Nucleus–Globus Pallidus Network. *J Neurosci* 30, 2010.

Humphries MD, **Stewart RD**, **Gurney KN**. A Physiologically Plausible Model of Action Selection and Oscillatory Activity in the Basal Ganglia. *J Neurosci* 26: 12921–12942, 2006.

Jávor-Duray BN, **Vinck M**, **van der Roest M**, **Mulder AB**, **Stam CJ**, **Berendse HW**, **Voorn P**. Early-onset cortico-cortical synchronization in the hemiparkinsonian rat model [Online]. *J Neurophysiol* 113, 2015. http://jn.physiology.org.libproxy.ucl.ac.uk/content/113/3/925 [24 Aug. 2017].

Kondabolu K, **Roberts EA**, **Bucklin M**, **McCarthy MM**, **Kopell N**, **Han X**. Striatal cholinergic interneurons generate beta and gamma oscillations in the corticostriatal circuit and produce motor deficits. *Proc Natl Acad Sci U S A* 113: E3159-68, 2016.

Koshimizu Y, **Fujiyama F**, **Nakamura KC**, **Furuta T**, **Kaneko T**. Quantitative analysis of axon bouton distribution of subthalamic nucleus neurons in the rat by single neuron visualization with a viral vector. *J Comp Neurol* 521: 2125–2146, 2013.

Kühn AA, **Kupsch A**, **Schneider G-H**, **Brown P**. Reduction in subthalamic 8-35 Hz oscillatory activity correlates with clinical improvement in Parkinson's disease. *Eur J Neurosci* 23: 1956–60, 2006.

Kumar A, **Cardanobile S**, **Rotter S**, **Aertsen A**. The role of inhibition in generating and controlling Parkinson's disease oscillations in the Basal Ganglia. *Front Syst Neurosci* 5: 86, 2011a.

Kumar A, **Cardanobile S**, **Rotter S**, **Aertsen A**. The Role of Inhibition in Generating and Controlling Parkinson?s Disease Oscillations in the Basal Ganglia. *Front Syst Neurosci* 5: 86, 2011b.

Lalo E, **Thobois S**, **Sharott A**, **Polo G**, **Mertens P**, **Pogosyan A**, **Brown P**. Patterns of Bidirectional Communication between Cortex and Basal Ganglia during Movement in Patients with Parkinson Disease. *J Neurosci* 28, 2008.

Lanciego JL, **Luquin N**, **Obeso JA**. Functional neuroanatomy of the basal ganglia. *Cold Spring Harb Perspect Med* 2: a009621, 2012.

Leblois A. Competition between Feedback Loops Underlies Normal and Pathological Dynamics in the Basal Ganglia. *J Neurosci* 26: 3567–3583, 2006.

Leblois A, **Boraud T**, **Meissner W**, **Bergman H**, **Hansel D**. Competition between Feedback Loops Underlies Normal and Pathological Dynamics in the Basal Ganglia. *J Neurosci* 26: 3567–3583, 2006.

Levy R. Dependence of subthalamic nucleus oscillations on movement and dopamine in Parkinson's disease. *Brain* 125: 1196–1209, 2002.

Levy R, **Hutchison WD**, **Lozano AM**, **Dostrovsky JO**. High-frequency Synchronization of Neuronal Activity in the Subthalamic Nucleus of Parkinsonian Patients with Limb Tremor [Online]. *J Neurosci* 20: 7766–7775, 2000. http://www.jneurosci.org/content/20/20/7766.full [21 Oct. 2015].

Lienard JF, **Cos I**, **Girard B**. Beta-Band Oscillations without Pathways: the opposing Roles of D2 and D5 Receptors. *doi.org* (July 10, 2017). doi: 10.1101/161661.

Litvak V, **Jha A**, **Eusebio A**, **Oostenveld R**, **Foltynie T**, **Limousin P**, **Zrinzo L**, **Hariz MI**, **Friston K**, **Brown P**. Resting oscillatory cortico-subthalamic connectivity in patients with Parkinson's disease. *Brain* 134: 359–374, 2011a.

Litvak V, **Jha A**, **Eusebio A**, **Oostenveld R**, **Foltynie T**, **Limousin P**, **Zrinzo L**, **Hariz MI**, **Friston K**, **Brown P**. Resting oscillatory cortico-subthalamic connectivity in patients with Parkinson's disease. *Brain* 134: 359–74, 2011b.

Liu C, **Zhu Y**, **Liu F**, **Wang J**, **Li H**, **Deng B**, **Fietkiewicz C**, **Loparo KA**. Neural mass models describing possible origin of the excessive beta oscillations correlated with Parkinsonian state. *Neural Networks* 88: 65–73, 2017.

López-Azcárate J, **Tainta M**, **Rodríguez-Oroz MC**, **Valencia M**, **González R**, **Guridi J**, **Iriarte J**, **Obeso JA**, **Artieda J**, **Alegre M**. Coupling between beta and high-frequency activity in the human subthalamic nucleus may be a pathophysiological mechanism in Parkinson's disease. *J Neurosci* 30: 6667–77, 2010.

Magill P., **Bolam J.**, **Bevan M.** Dopamine regulates the impact of the cerebral cortex on the subthalamic nucleus–globus pallidus network. *Neuroscience* 106: 313–330, 2001.

Magill PJ, **Pogosyan A**, **Sharott A**, **Csicsvari J**, **Bolam JP**, **Brown P**. Changes in functional connectivity within the rat striatopallidal axis during global brain activation in vivo. *J Neurosci* 26: 6318–6329, 2006.

Magill PJ, **Sharott A**, **Bolam JP**, **Brown P**. Brain State–Dependency of Coherent Oscillatory Activity in the Cerebral Cortex and Basal Ganglia of the Rat [Online]. *J Neurophysiol* 92, 2004. http://jn.physiology.org/content/92/4/2122.full [26 Apr. 2017].

Mallet N, **Micklem BR**, **Henny P**, **Brown MT**, **Williams C**, **Bolam JP**, **Nakamura KC**, **Magill PJ**. Dichotomous Organization of the External Globus Pallidus. *Neuron* 74: 1075–1086, 2012.

Mallet N, **Pogosyan A**, **Marton LF**, **Bolam JP**, **Brown P**, **Magill PJ**. Parkinsonian Beta Oscillations in the External Globus Pallidus and Their Relationship with Subthalamic Nucleus Activity. *J Neurosci* 28: 14245–14258, 2008a.

Mallet N, **Pogosyan A**, **Sharott A**, **Csicsvari J**, **Bolam JP**, **Brown P**, **Magill PJ**. Disrupted Dopamine Transmission and the Emergence of Exaggerated Beta Oscillations in Subthalamic Nucleus and Cerebral Cortex. *J Neurosci* 28: 4795–4806, 2008b.

Marceglia S, **Foffani G**, **Bianchi AM**, **Baselli G**, **Tamma F**, **Egidi M**, **Priori A**. Dopamine-dependent non-linear correlation between subthalamic rhythms in Parkinson's disease. *J Physiol* 571: 579–591, 2006.

Maris E. Statistical testing in electrophysiological studies. *Psychophysiology* 49: 549–565, 2012.

Maris E, **Oostenveld R**. Nonparametric statistical testing of EEG- and MEG-data. *J Neurosci Methods* 164: 177–190, 2007.

Marreiros AC, **Cagnan H**, **Moran RJ**, **Friston KJ**, **Brown P**. Basal ganglia–cortical interactions in Parkinsonian patients. *Neuroimage* 66: 301–310, 2013.

Matias FS, **Carelli P V.**, **Mirasso CR**, **Copelli M**. Anticipated synchronization in a biologically plausible model of neuronal motifs. *Phys Rev E* 84: 21922, 2011.

McCarthy MM, **Moore-Kochlacs C**, **Gu X**, **Boyden ES**, **Han X**, **Kopell N**. Striatal origin of the pathologic beta oscillations in Parkinson's disease. *Proc Natl Acad Sci U S A* 108: 11620–5, 2011.

McHaffie JG, **Stanford TR**, **Stein BE**, **Coizet V**, **Redgrave P**. Subcortical loops through the basal ganglia. *Trends Neurosci* 28: 401–407, 2005.

Medkour T, **Walden AT**, **Burgess A**. Graphical modelling for brain connectivity via partial coherence. *J Neurosci Methods* 180: 374–383, 2009.

van der Meer M, **Kalenscher T**, **Lansink CS**, **Pennartz C**, **Berke JD**, **Redish AD**. Integrating early results on ventral striatal gamma oscillations in the rat. *Front Neurosci* 4: 300, 2010.

Moran RJ, **Mallet N**, **Litvak V**, **Dolan RJ**, **Magill PJ**, **Friston KJ**, **Brown P**. Alterations in brain connectivity underlying beta oscillations in parkinsonism. *PLoS Comput Biol* 7: e1002124, 2011.

Nambu A, **Tokuno H**, **Takada M**. Functional significance of the cortico–subthalamo–pallidal "hyperdirect" pathway. *Neurosci Res* 43: 111–117, 2002.

Nevado-Holgado AJ, **Mallet N**, **Magill PJ**, **Bogacz R**. Effective connectivity of the subthalamic

nucleus - globus pallidus network during Parkinsonian oscillations. *J Physiol* 7: 1429–1455, 2014.

Ni Z, **Bouali-Benzzouz R**, **Gao D**, **Benabid A-L**, **Benazzouz A**. Changes in the firing pattern of globus pallidus neurons after the degenration of nigrostriatal pathway are mediated by the subthalamic nucleus in the rat. *Eur J Neurosci* 12: 4338–4344, 2000.

Nicolás MJ, **López-Azcárate J**, **Valencia M**, **Alegre M**, **Pérez-Alcázar M**, **Iriarte J**, **Artieda J**. Ketamine-Induced Oscillations in the Motor Circuit of the Rat Basal Ganglia. *PLoS One* 6: e21814, 2011.

Nolte G, **Bai O**, **Wheaton L**, **Mari Z**, **Vorbach S**, **Hallett M**. Identifying true brain interaction from EEG data using the imaginary part of coherency. *Clin Neurophysiol* 115: 2292–307, 2004.

Oostenveld R, **Fries P**, **Maris E**, **Schoffelen J-M**, **Oostenveld R**, **Fries P**, **Maris E**, **Schoffelen J-M**. FieldTrip: Open Source Software for Advanced Analysis of MEG, EEG, and Invasive Electrophysiological Data. *Comput Intell Neurosci* 2011: 1–9, 2011.

Oswal A, **Beudel M**, **Zrinzo L**, **Limousin P**, **Hariz M**, **Foltynie T**, **Litvak V**, **Brown P**. Deep brain stimulation modulates synchrony within spatially and spectrally distinct resting state networks in Parkinson's disease. *Brain* 139: 1482–1496, 2016.

Parker PRL, **Lalive AL**, **Kreitzer AC**. Pathway-Specific Remodeling of Thalamostriatal Synapses in Parkinsonian Mice. *Neuron* 89: 734–740, 2016.

Pavlides A, **Hogan SJ**, **Bogacz R**. Computational Models Describing Possible Mechanisms for Generation of Excessive Beta Oscillations in Parkinson's Disease. *PLOS Comput Biol* 11: e1004609, 2015.

Pavlides A, **John Hogan S**, **Bogacz R**. Improved conditions for the generation of beta oscillations in the subthalamic nucleus-globus pallidus network. *Eur J Neurosci* 36: 2229–2239, 2012.

Paxinos G, **Watson C**. *The rat brain in stereotaxic coordinates*. Elsevier, 2007.

Plenz D, **Kital ST**. A basal ganglia pacemaker formed by the subthalamic nucleus and external globus pallidus. *Nature* 400: 677–82, 1999.

Priori A, **Foffani G**, **Pesenti A**, **Tamma F**, **Bianchi AM**, **Pellegrini M**, **Locatelli M**, **Moxon KA**, **Villani RM**. Rhythm-specific pharmacological modulation of subthalamic activity in Parkinson's disease. *Exp Neurol* 189: 369–79, 2004.

Qiu C, **Shivacharan RS**, **Zhang M**, **Durand DM**. Can Neural Activity Propagate by Endogenous Electrical Field? *J Neurosci* 35: 15800–11, 2015.

Ray NJ, **Jenkinson N**, **Wang S**, **Holland P**, **Brittain JS**, **Joint C**, **Stein JF**, **Aziz T**. Local field

potential beta activity in the subthalamic nucleus of patients with Parkinson's disease is associated with improvements in bradykinesia after dopamine and deep brain stimulation. *Exp Neurol* 213: 108–113, 2008.

Rosenberg JR, **Halliday DM**, **Breeze P**, **Conway BA**. Identification of patterns of neuronal connectivity—partial spectra, partial coherence, and neuronal interactions. *J Neurosci Methods* 83: 57–72, 1998.

Salvador R, **Suckling J**, **Schwarzbauer C**, **Bullmore E**. Undirected graphs of frequency-dependent functional connectivity in whole brain networks. *Philos Trans R Soc Lond B Biol Sci* 360: 937–46, 2005.

Sato F, **Parent M**, **Levesque M**, **Parent A**. Axonal branching pattern of neurons of the subthalamic nucleus in primates. *J Comp Neurol* 424: 142–152, 2000.

Schnitzler A, **Gross J**. Normal and pathological oscillatory communication in the brain. *Nat Rev Neurosci* 6: 285–96, 2005.

Schoffelen J-M, **Oostenveld R**, **Fries P**. Neuronal coherence as a mechanism of effective corticospinal interaction. *Science* 308: 111–113, 2005.

Schroll H, **Hamker FH**. Computational models of basal-ganglia pathway functions: focus on functional neuroanatomy. *Front Syst Neurosci* 7: 1–18, 2013.

Schroll H, **Vitay J**, **Hamker FH**. Dysfunctional and compensatory synaptic plasticity in Parkinson's disease. *Eur J Neurosci* 39: 688–702, 2014.

Schwarting RK, **Huston JP**. Unilateral 6-hydroxydopamine lesions of meso-striatal dopamine neurons and their physiological sequelae. [Online]. *Prog Neurobiol* 49: 215–66, 1996a. http://www.ncbi.nlm.nih.gov/pubmed/8878304 [28 Apr. 2017].

Schwarting RK, **Huston JP**. The unilateral 6-hydroxydopamine lesion model in behavioral brain research. Analysis of functional deficits, recovery and treatments. [Online]. *Prog Neurobiol* 50: 275–331, 1996b. http://www.ncbi.nlm.nih.gov/pubmed/8971983 [28 Apr. 2017].

Sharott A, **Gulberti A**, **Zittel S**, **Tudor Jones AA**, **Fickel U**, **Münchau A**, **Köppen JA**, **Gerloff C**, **Westphal M**, **Buhmann C**, **Hamel W**, **Engel AK**, **Moll CKE**. Activity Parameters of Subthalamic Nucleus Neurons Selectively Predict Motor Symptom Severity in Parkinson's Disease [Online]. *J Neurosci* 34, 2014. http://www.jneurosci.org.libproxy.ucl.ac.uk/content/34/18/6273 [24 Aug. 2017].

Sharott A, **Magill PJ**, **Bolam JP**, **Brown P**. Directional analysis of coherent oscillatory field potentials in the cerebral cortex and basal ganglia of the rat. *J Physiol* 562: 951–63, 2005a.

Sharott A, **Magill PJ**, **Harnack D**, **Kupsch A**, **Meissner W**, **Brown P**. Dopamine depletion

1139 increases the power and coherence of beta-oscillations in the cerebral cortex and subthalamic nucleus
1140 of the awake rat. *Eur J Neurosci* 21: 1413–1422, 2005b.

1141 **Sharott A**, **Moll CKE**, **Engler G**, **Denker M**, **Grün S**, **Engel AK**. Different Subtypes of Striatal
1142 Neurons Are Selectively Modulated by Cortical Oscillations [Online]. *J Neurosci* 29, 2009.
1143 http://www.jneurosci.org/content/29/14/4571.long [24 Jul. 2017].

1144 **Sharott A**, **Vinciati F**, **Nakamura KC**, **Magill PJ**. A Population of Indirect Pathway Striatal
1145 Projection Neurons Is Selectively Entrained to Parkinsonian Beta Oscillations. *J Neurosci* 37: 9977–
1146 9998, 2017.

1147 **Shen W**, **Flajolet M**, **Greengard P**, **Surmeier DJ**. Dichotomous Dopaminergic Control of Striatal
1148 Synaptic Plasticity [Online]. *Science (80-)* 321, 2008.
1149 http://science.sciencemag.org/content/321/5890/848.long [23 Jun. 2017].

1150 **Shouno O**, **Tachibana Y**, **Nambu A**, **Doya K**. Computational Model of Recurrent Subthalamo-
1151 Pallidal Circuit for Generation of Parkinsonian Oscillations. *Front Neuroanat* 11: 21, 2017.

1152 **Smith Y**, **Bevan MD**, **Shink E**, **Bolam JP**. Microcircuitry of the direct and indirect pathways of the
1153 basal ganglia. *Neuroscience* 86: 353–387, 1998.

1154 **Smith Y**, **Galvan A**, **Ellender TJ**, **Doig N**, **Villalba RM**, **Huerta-Ocampo I**, **Wichmann T**, **Bolam**
1155 **JP**. The thalamostriatal system in normal and diseased states. *Front Syst Neurosci* 8: 5, 2014.

1156 **Stam CJ**, **Nolte G**, **Daffertshofer A**. Phase lag index: Assessment of functional connectivity from
1157 multi channel EEG and MEG with diminished bias from common sources. *Hum Brain Mapp* 28:
1158 1178–1193, 2007.

1159 **Steriade M**. Corticothalamic resonance, states of vigilance and mentation. *Neuroscience* 101: 243–
1160 276, 2000.

1161 **Tachibana Y**, **Iwamuro H**, **Kita H**, **Takada M**, **Nambu A**. Subthalamo-pallidal interactions
1162 underlying parkinsonian neuronal oscillations in the primate basal ganglia. *Eur J Neurosci* 34: 1470–
1163 1484, 2011.

1164 **Terman D**, **Rubin JE**, **Yew AC**, **Wilson CJ**. Activity patterns in a model for the subthalamopallidal
1165 network of the basal ganglia. *J Neurosci* 22: 2963–2976, 2002.

1166 **Thut G**, **Miniussi C**, **Gross J**. The functional importance of rhythmic activity in the brain. *Curr Biol*
1167 22: R658-63, 2012.

1168 **Tseng KY**, **Kasanetz F**, **Kargieman L**, **Riquelme LA**, **Murer MG**. Cortical Slow Oscillatory
1169 Activity Is Reflected in the Membrane Potential and Spike Trains of Striatal Neurons in Rats with
1170 Chronic Nigrostriatal Lesions [Online]. *J Neurosci* 21, 2001.

http://www.jneurosci.org/content/21/16/6430.long [2 May 2017].

Uhlhaas PJ, **Singer W**. Neural Synchrony in Brain Disorders: Relevance for Cognitive Dysfunctions and Pathophysiology. *Neuron* 52: 155–168, 2006.

Varela F, **Lachaux J-PP**, **Rodriguez E**, **Martinerie J**. The brainweb: phase synchronization and large-scale integration. *Nat Rev Neurosci* 2: 229–39, 2001.

Vicente R, **Gollo LL**, **Mirasso CR**, **Fischer I**, **Pipa G**. Dynamical relaying can yield zero time lag neuronal synchrony despite long conduction delays. *Proc Natl Acad Sci U S A* 105: 17157–62, 2008.

Vinck M, **Oostenveld R**, **van Wingerden M**, **Battaglia F**, **Pennartz CMA**. An improved index of phase-synchronization for electrophysiological data in the presence of volume-conduction, noise and sample-size bias. *Neuroimage* 55: 1548–1565, 2011.

Viriyopase A, **Bojak I**, **Zeitler M**, **Gielen S**. When Long-Range Zero-Lag Synchronization is Feasible in Cortical Networks. *Front Comput Neurosci* 6: 49, 2012.

Weinberger M, **Mahant N**, **Hutchison WD**, **Lozano AM**, **Moro E**, **Hodaie M**, **Lang AE**, **Dostrovsky JO**. Beta oscillatory activity in the subthalamic nucleus and its relation to dopaminergic response in Parkinson's disease. *J Neurophysiol* 96: 3248–56, 2006.

West T, **Farmer S**, **Berthouze L**, **Jha A**, **Beudel M**, **Foltynie T**, **Limousin P**, **Zrinzo L**, **Brown P**, **Litvak V**. The Parkinsonian Basal Ganglia Network: Measures of Power, Linear and Non-Linear Synchronization and their Relationship to L-DOPA Treatment and OFF State Motor Severity. *Front Hum Neurosci* 10: 517, 2016.

Whitmer D, **de Solages C**, **Hill B**, **Yu H**, **Henderson JM**, **Bronte-Stewart H**. High frequency deep brain stimulation attenuates subthalamic and cortical rhythms in Parkinson's disease. *Front Hum Neurosci* 6: 155, 2012.

Wichmann T, **DeLong MR**. Neurobiology: Oscillations in the basal ganglia. *Nature* 400: 621–622, 1999.

van Wijk BCM, **Neumann W-J**, **Schneider G-H**, **Sander TH**, **Litvak V**, **Kühn AA**. Low-beta cortico-pallidal coherence decreases during movement and correlates with overall reaction time. *Neuroimage* (2017). doi: 10.1016/j.neuroimage.2017.07.024.

Wilson CJ. Active decorrelation in the basal ganglia. *Neuroscience* 250: 467–482, 2013.

Zold CL, **Kasanetz F**, **Pomata PE**, **Belluscio MA**, **Escande M V**, **Galinanes GL**, **Riquelme LA**, **Murer MG**. Striatal gating through up states and oscillations in the basal ganglia: Implications for Parkinson's disease. *J Physiol Paris* 106: 40–6, 2012.

Figure Legends:

Figure 1 – **Cortical-basal ganglia circuits and experimental paradigm. (A)** Schematic of canonical cortical-basal ganglia circuit incorporating the antagonistic direct and indirect pathways first described by Albin et al. (1989), as well as the cortico-subthalamic hyperdirect pathway (Nambu et al., 2002). The motor cortex (M2, purple) has major inputs to the basal ganglia at the striatum (STR, green) and subthalamic nucleus (STN, red). Information flow along the indirect pathway is routed via the external segment of the globus pallidus (GPe, Orange). Both indirect, direct and hyperdirect pathways ultimately impinge upon the output nuclei of the basal ganglia, made up of the entopeduncular nucleus (EPN) and substantia nigra pars reticulata (SNr). BG output targets thalamic relays, of which some return back to motor cortex. Brain structures from which neuronal signals were recorded in this study are delineated by solid boxes, with solid arrows indicating their connections (interactions) that were analyzed here. Other structures and interactions are respctively delineated by dashed boxes and arrows. **(B)** Diagram of the recording configuration in anaesthetised rats. Local field potentials (LFPs) were recorded from the BG using two multi-channel 'silicon probes'; the first probe was targeted to the STR and GPe, whereas the second probe was targeted to STN. Electrocorticograms (ECoG) were recorded with a screw positioned over the "secondary motor cortex" (M2). Boundaries and positioning are approximate.

Figure 2 - **Example recordings of subcortical monopolar LFP and cortical ECoG signals for a single animal from either the control (A-B), or the 6-OHDA lesioned (C-D) groups. (A)** 100 second sample of LFPs recording made from one dopamine intact, control animal. The example trace shows the time course of LFP recordings recorded using silicon electrodes implanted in the external globus pallidus (GPe), striatum (STR) and subthalamic nucleus (STN). Additionally, ECoG was recorded from a screw positioned over motor cortex (M2). Only raw data is shown. The data was de-meaned and then high pass filtered at 4Hz. **(B)** Spectral analysis of example control animal's recording. Data was epoched into 1-second long segments, those contaminated by muscle artefact or high amplitude transients were removed using Z-thresholding as described in the text. These epochs were used to construct individual FFTs and subsequent periodograms. **(C)** Same as (A) but for an example 6-OHDA, dopamine depleted animal. The dashed line shows a regression to estimate the 1/f background noise. **(D)** Same as (B) but for 6-OHDA lesioned animal.

Figure 3 – **Group averaged power spectra for all rats across both control and lesion conditions.** Spectra are shown for signals recorded from **(A)** motor cortex (M2), **(B)** the striatum (STR), **(C)** the subthalamic nucleus (STN), and **(D)** the external globus pallidus (GPe). The group averages for either the 6-OHDA dopamine depleted or control animals are shown by bold lines in red or blue respectively. Shading shows the mean ±1 S.E.M. Results of cluster permutation tests for the effect of the lesion are indicated by the black bar and corresponding P-value. All recording sites presented beta

peaks around 18-20 Hz. Cluster based permutation testing for significant differences between conditions showed that there was a significant increase in beta in the lesioned animals for signals at all recorded sites. The dashed lines indicate a linear regression in log-log space as a rough estimate to the 1/f backgroung.

Figure 4 – **Functional connectivity estimates using imaginary part of coherence (iCOH).** Spectra for each animal are shown by thin lines corresponding to either 6-OHDA lesioned (blue) or control (red). The group averages for either the 6-OHDA dopamine depleted or control animals are shown by bold lines in red or blue respectively. Shading shows the mean ±1 S.E.M. Cluster-based permutation statistics were applied to test the effect of the lesion. Significant clusters are indicated by the black line above the spectra and corresponding P-value. The iCOH metric, robust to zero-lag interactions, presents a richer view of functional connectivity that would otherwise be missed if using standard coherence (data not shown). Beta activity is predominant across all cross-regional pairings. STN and GPe also show intra-nuclear correlations in this range in the dopamine depleted state. Notably there is also a high beta/gamma interaction between STN/M2 and STN/STR that is visible in both control and lesion animals.

Figure 5 - **Directed connectivity estimated using non-parametric directionality (NPD) between subcortically recorded LFPs (GPe, STN, and STR) and ECoG recorded at motor cortex (M2).** NPD decomposes the coherence between pairs of signals into forward and reverse components. The array of spectra in the figures reads such that each row title gives the structure with a forward coherence targeted to the structure given by the name given above the column. The group averages for either the 6-OHDA dopamine depleted or control animals are shown by bold lines in red or blue respectively. Shading shows the mean ±1 S.E.M. Cluster-based permutation statistics were applied to test the effect of the lesion. Significant clusters are indicated by the black line above the spectra and corresponding P-value.

Figure 6 - **Non-parametric directionality conditioned on the STN local field potential -** Spectra for each animal are shown by thin lines corresponding to either 6-OHDA lesioned (blue) or control (red). The group averages for either the 6-OHDA dopamine depleted or control animals are shown by bold lines in red or blue respectively. Shading shows the mean ±1 S.E.M. Cluster-based permutation statistics were applied to test the effect of the lesion. Significant clusters are indicated by the black line above the spectra and corresponding P-value. The effect of conditioning with the STN LFP was also tested using cluster permutation statistics. Frequencies where NPD was significantly attenuated by the conditioning are indicated by the red and blue bars (and corresponding P-values) for the control and lesion recordings respectively.

Figure 7 - **Non-parametric directionality conditioned on the GPe local field potential -** Spectra for each animal are shown by thin lines corresponding to either 6-OHDA lesioned (blue) or control (red).

The group averages for either the 6-OHDA dopamine depleted or control animals are shown by bold lines in red or blue respectively. Shading shows the mean ±1 S.E.M. Cluster-based permutation statistics were applied to test the effect of the lesion. Significant clusters are indicated by the black line above the spectra and corresponding P-value. The effect of conditioning with the GPe LFP was also tested using cluster permutation statistics. Frequencies where NPD was significantly attenuated by the conditioning are indicated by the red and blue bars (and corresponding P-values) for the control and lesion recordings respectively.

Figure 8 - **Non-parametric directionality conditioned on the STR local field potential -** Spectra for each animal are shown by thin lines corresponding to either 6-OHDA lesioned (blue) or control (red). The group averages for either the 6-OHDA dopamine depleted or control animals are shown by bold lines in red or blue respectively. Shading shows the mean ±1 S.E.M. Cluster-based permutation statistics were applied to test the effect of the lesion. Significant clusters are indicated by the black line above the spectra and corresponding P-value. The effect of conditioning with the STR LFP was also tested using cluster permutation statistics. Frequencies where NPD was significantly attenuated by the conditioning are indicated by the red and blue bars (and corresponding P-values) for the control and lesion recordings respectively.

Figure 9 - **Non-parametric directionality conditioned on the M2 electrocorticogram -** Spectra for each animal are shown by thin lines corresponding to either 6-OHDA lesioned (blue) or control (red). The group averages for either the 6-OHDA dopamine depleted or control animals are shown by bold lines in red or blue respectively. Shading shows the mean ±1 S.E.M. Cluster-based permutation statistics were applied to test the effect of the lesion. Significant clusters are indicated by the black line above the spectra and corresponding P-value. The effect of conditioning with the M2 ECoG was also tested using cluster permutation statistics. Frequencies where NPD was significantly attenuated by the conditioning are indicated by the red and blue bars (and corresponding P-values) for the control and lesion recordings respectively.

Table 1– **Summary of hypotheses of the impact of dopamine depletion on the propagation of beta rhythms in the cortico-basal ganglia circuit.**

Table 2 – **Summary of hypotheses for gamma flow in the cortico-basal ganglia circuit**

1305

1306

1307

1308

1309

1310

1311

1312

1313

1314

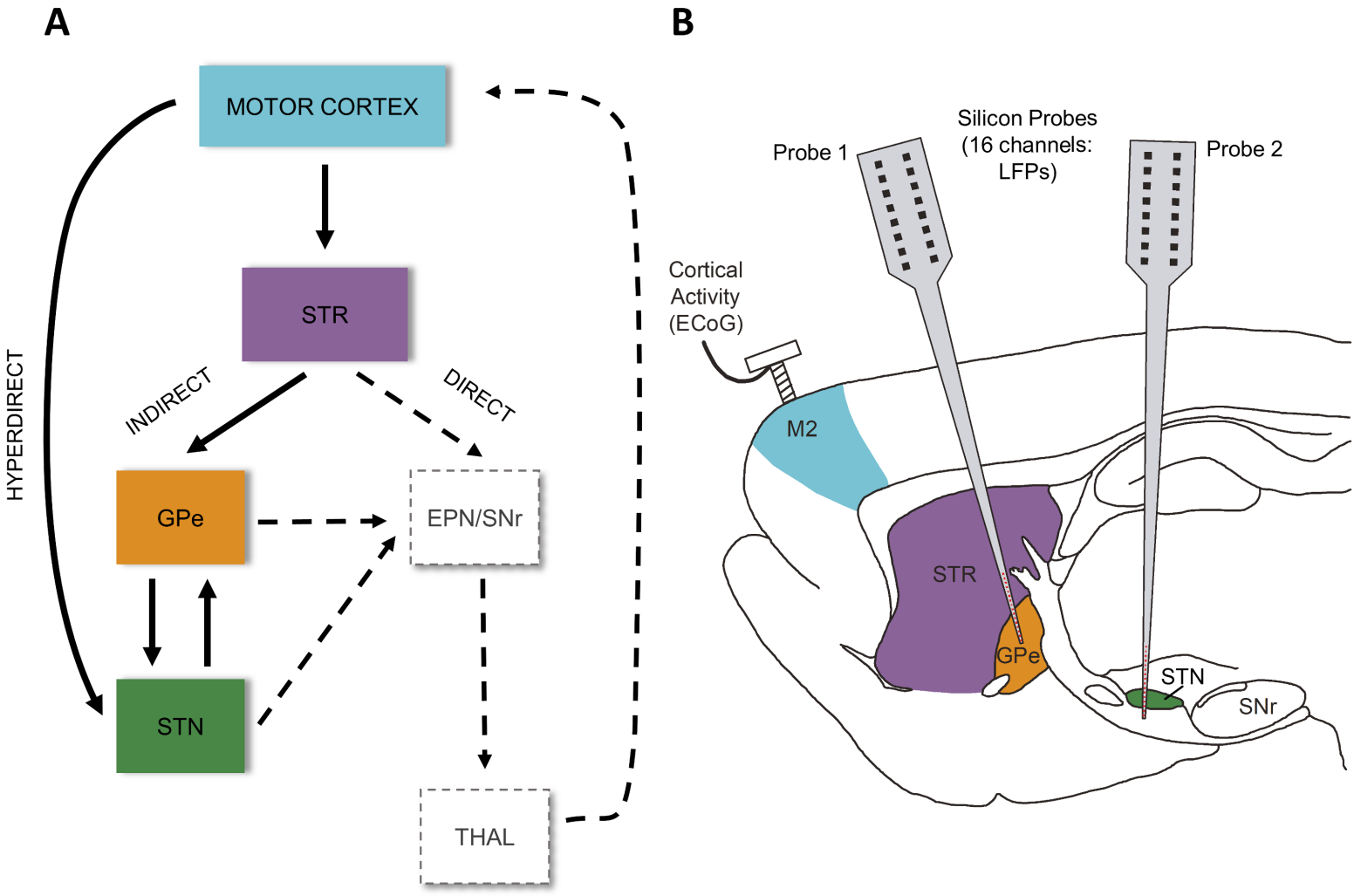
A
MOTOR CORTEX
STR
INDIRECT
DIRECT
HYPERDIRECT
GPe
EPN/SNr
STN
THAL
B
Silicon Probes
(16 channels:
LFPs)
Probe 1
Probe 2
Cortical
Activity
(ECoG)
M2
STR
GPe
STN
SNr

A

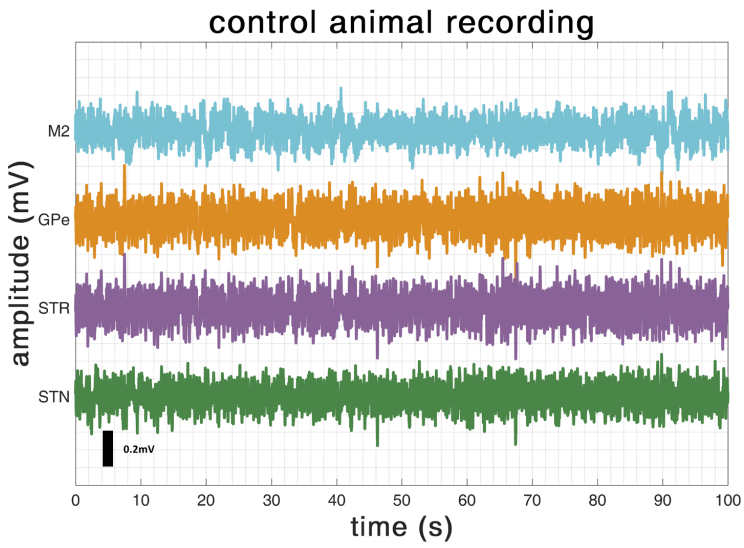
control animal recording
M2
GPe
STR
STN
amplitude (mV)
0.2mV
0
10
20
30
40
50
60
70
80
90
100
time (s)

B

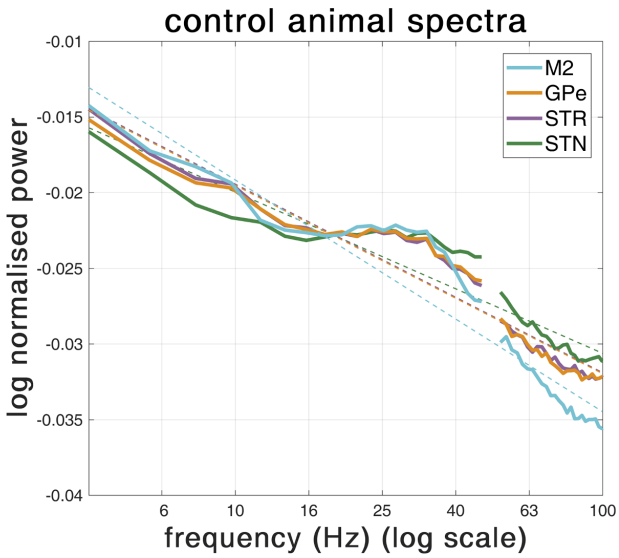
control animal spectra
M2
GPe
STR
STN
log normalised power
-0.01
-0.015
-0.02
-0.025
-0.03
-0.035
-0.04
6
10
16
25
40
63
100
frequency (Hz) (log scale)

C

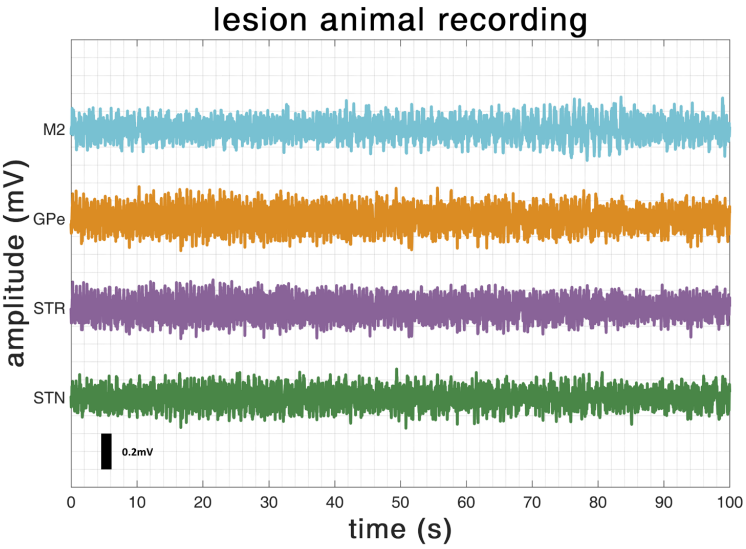
lesion animal recording
M2
GPe
STR
STN
amplitude (mV)
0.2mV
0
10
20
30
40
50
60
70
80
90
100
time (s)

D

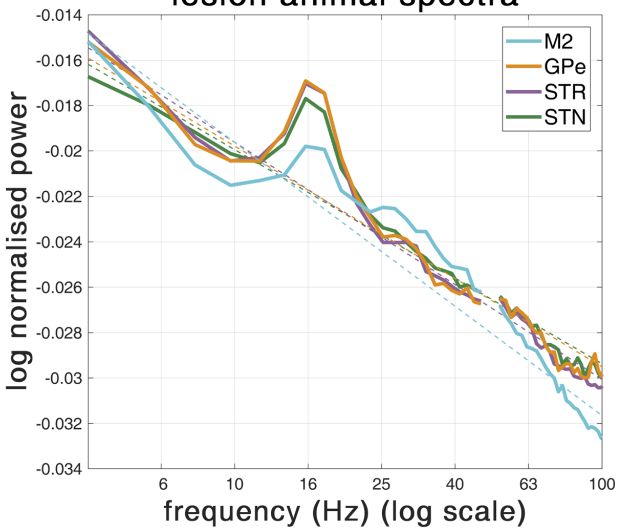
lesion animal spectra
M2
GPe
STR
STN
log normalised power
-0.014
-0.016
-0.018
-0.02
-0.022
-0.024
-0.026
-0.028
-0.03
-0.032
-0.034
6
10
16
25
40
63
100
frequency (Hz) (log scale)

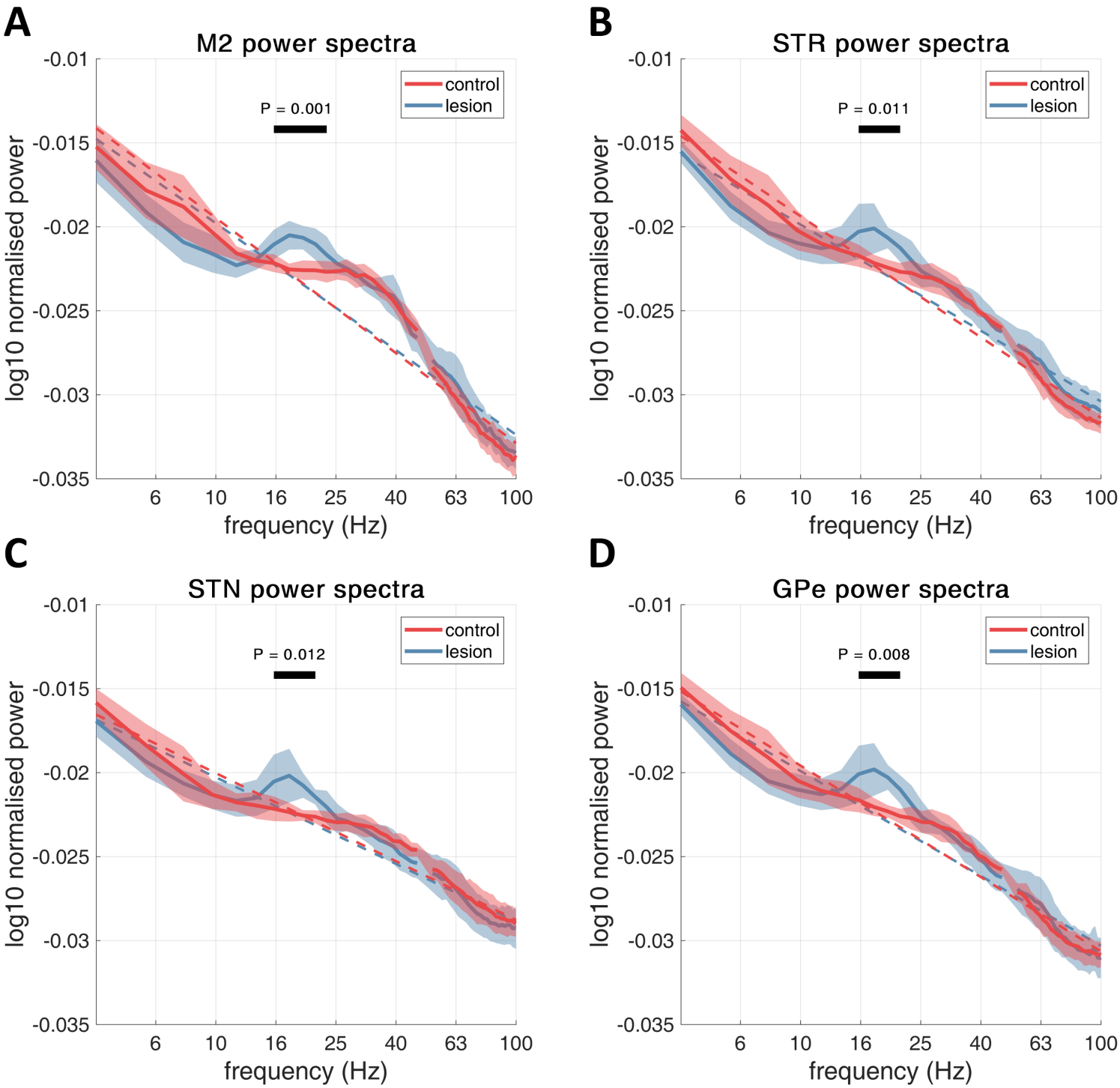
A
M2 power spectra
control
lesion
P = 0.001
log10 normalised power
-0.01
-0.015
-0.02
-0.025
-0.03
-0.035
6
10
16
25
40
63
100
frequency (Hz)
B
STR power spectra
control
lesion
P = 0.011
log10 normalised power
frequency (Hz)
C
STN power spectra
control
lesion
P = 0.012
log10 normalised power
frequency (Hz)
D
GPe power spectra
control
lesion
P = 0.008
log10 normalised power
frequency (Hz)

Imaginary Coherence

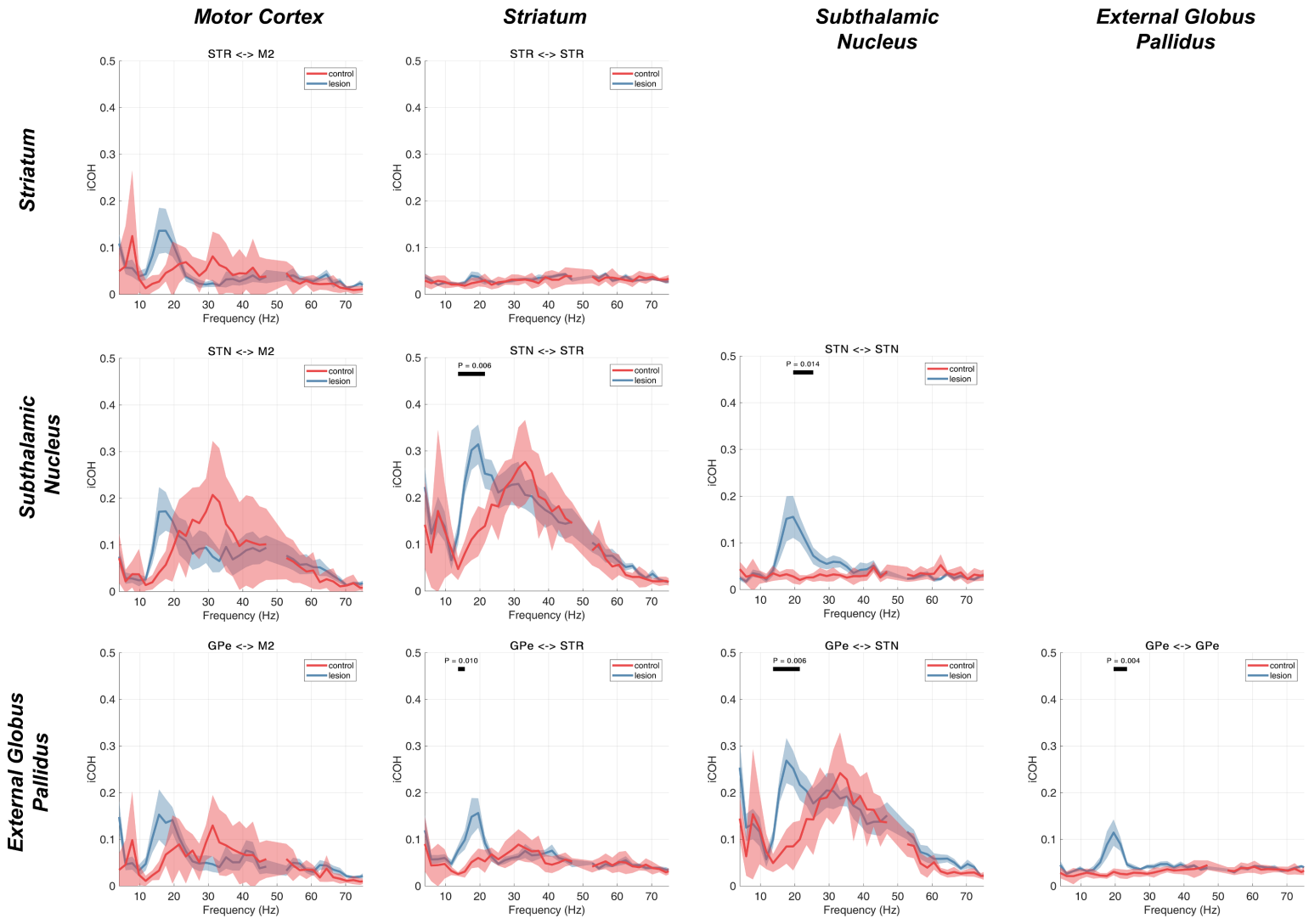

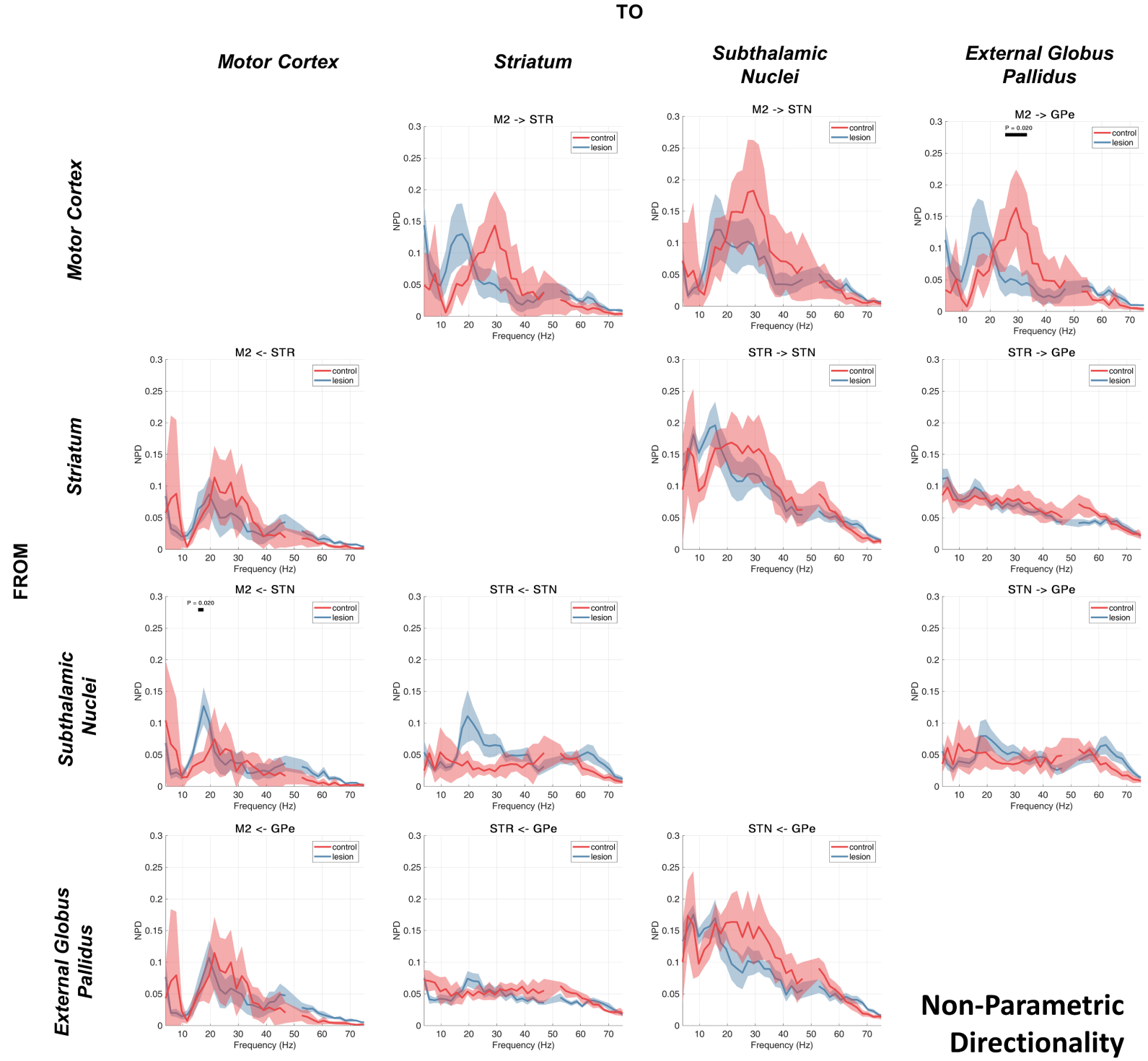
TO
FROM
Motor Cortex
Striatum
Subthalamic Nuclei
External Globus Pallidus
M2 -> STR
M2 -> STN
M2 -> GPe
M2 <- STR
STR -> STN
STR -> GPe
M2 <- STN
STR <- STN
STN -> GPe
M2 <- GPe
STR <- GPe
STN <- GPe
P = 0.020
control
lesion
NPD
Frequency (Hz)
Non-Parametric Directionality

FROM

TO

	Motor Cortex	Striatum	External Globus Pallidus
Motor Cortex		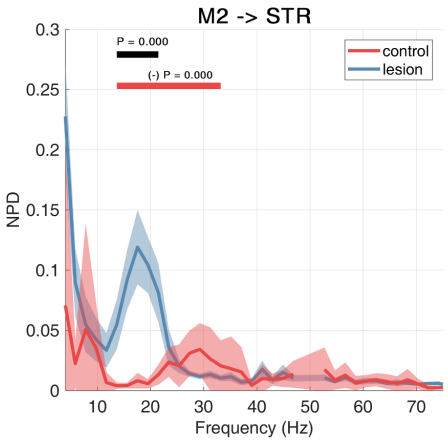	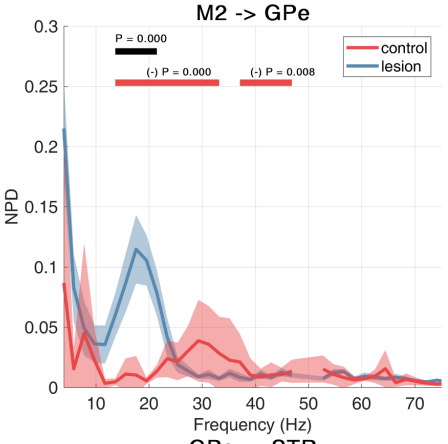
Striatum	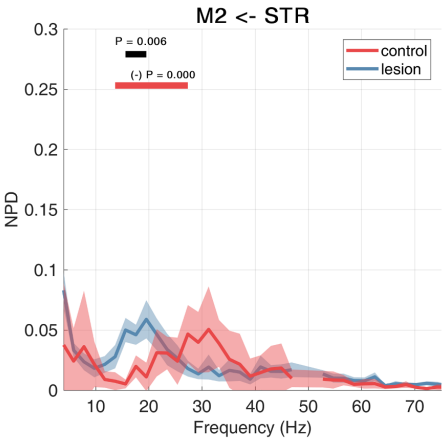		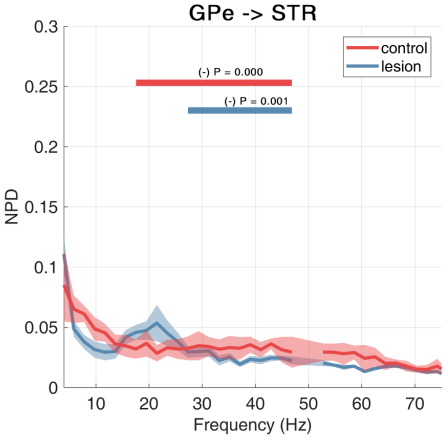
External Globus Pallidus	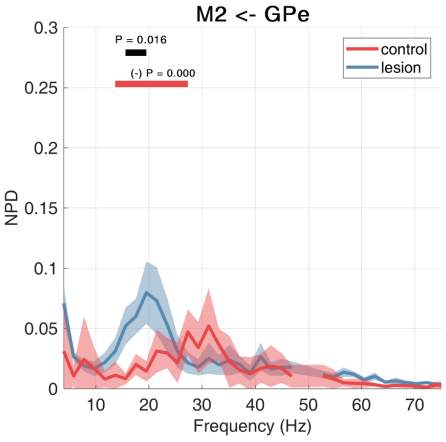	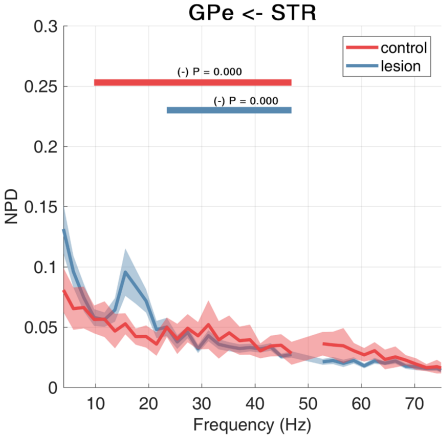	

STN conditioned Non-Parametric Directionality

TO

FROM

Motor Cortex | ***Striatum*** | ***Subthalamic Nucleus***

Motor Cortex

Striatum

Subthalamic Nucleus

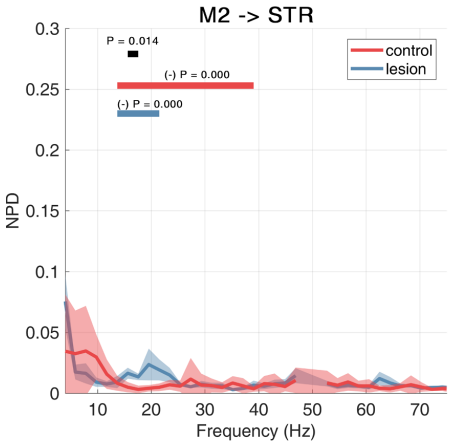

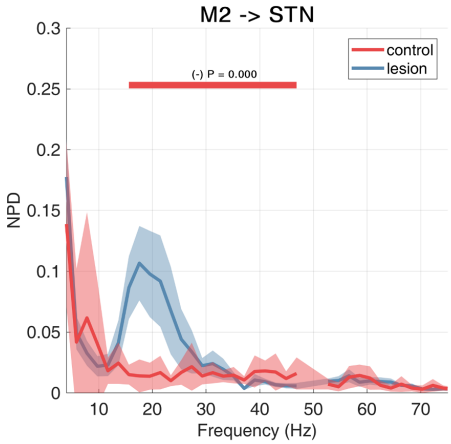

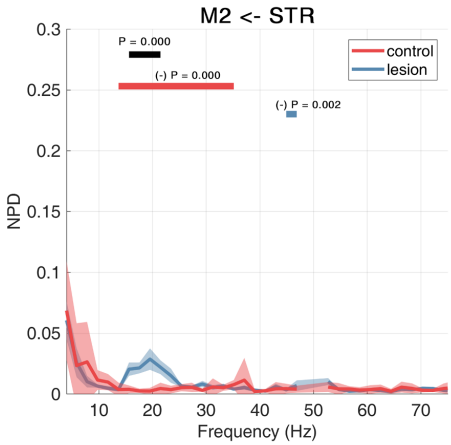

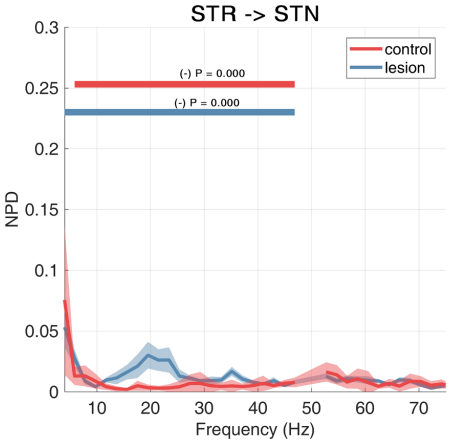

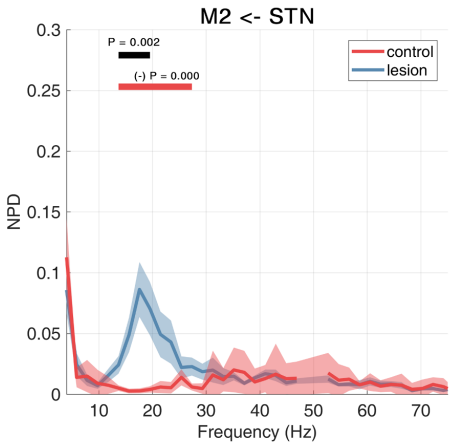

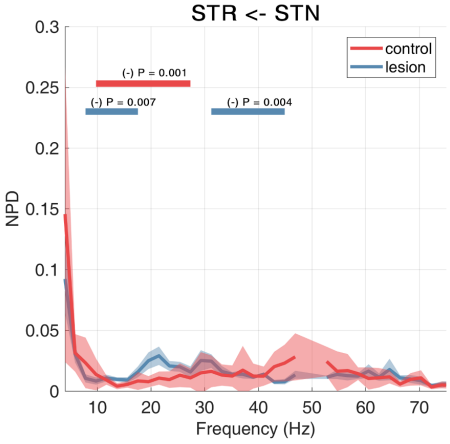

GPe conditioned Non-Parametric Directionality

TO

FROM

	Motor Cortex	***Subthalamic Nucleus***	***External Globus Pallidus***
Cortex		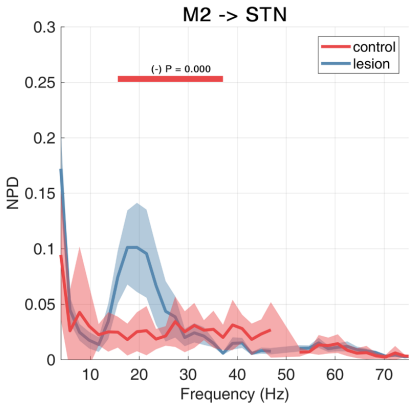	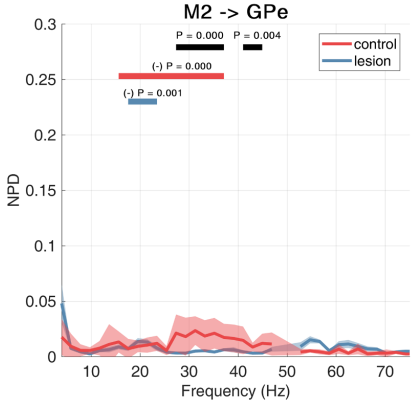
Subthalamic Nucleus	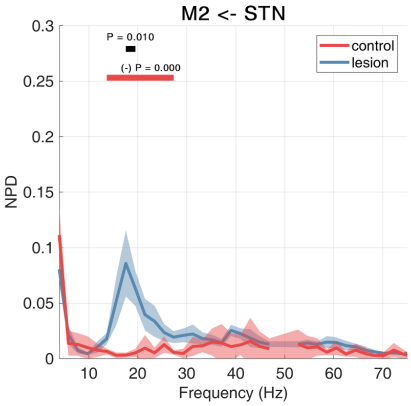		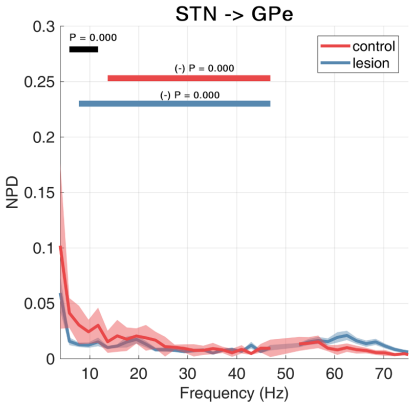
External Globus Pallidus	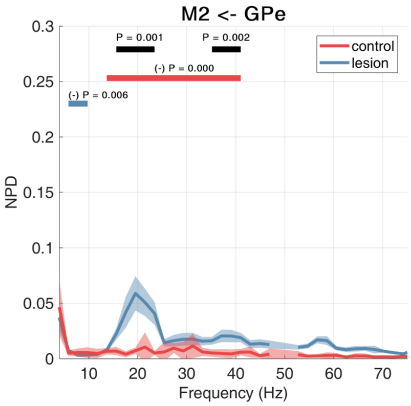	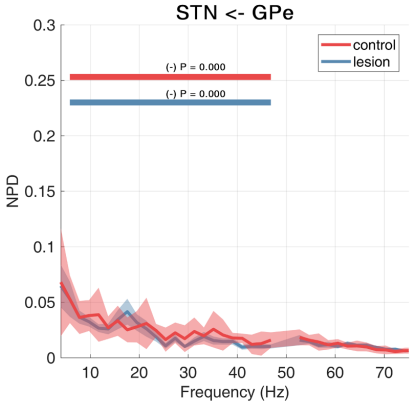	

STR conditioned Non-Parametric Directionality

TO

FROM

	Striatum	Subthalamic Nucleus	External Globus Pallidus
Striatum		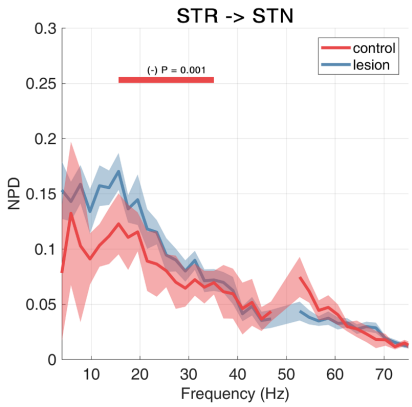	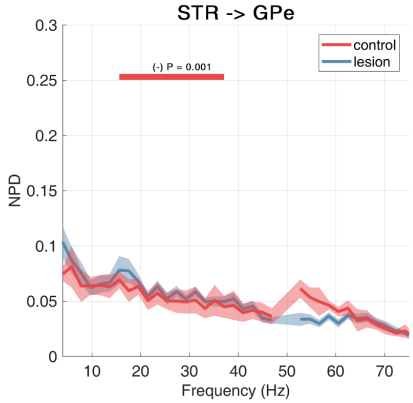
Subthalamic Nucleus	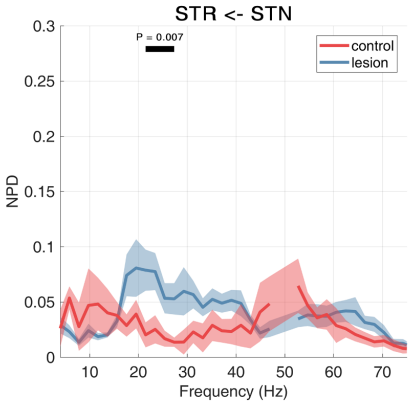		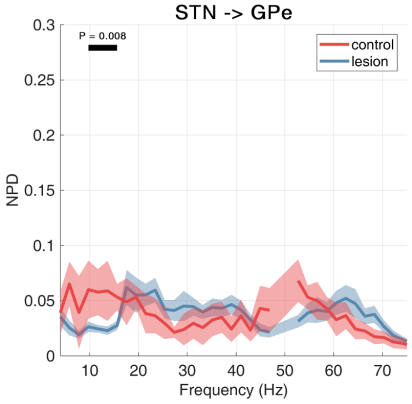
External Globus Pallidus	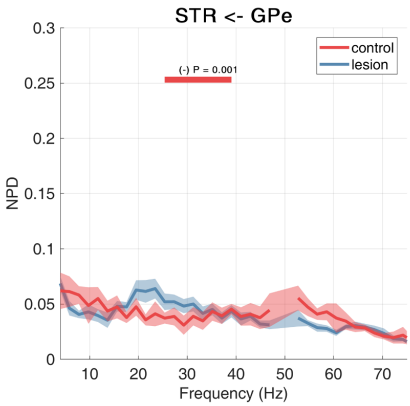	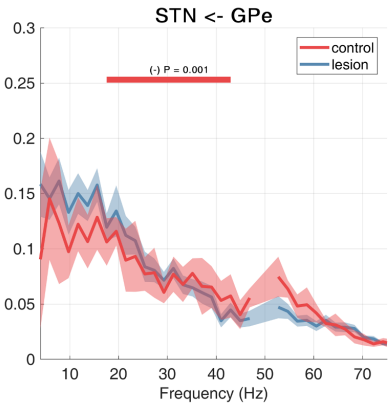	

M2 conditioned Non-Parametric Directionality

Hypotheses for propagation of low beta rhythms

	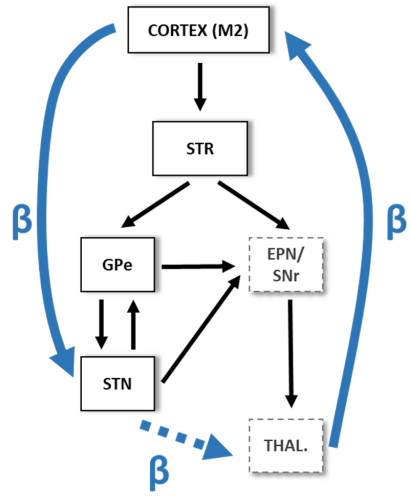	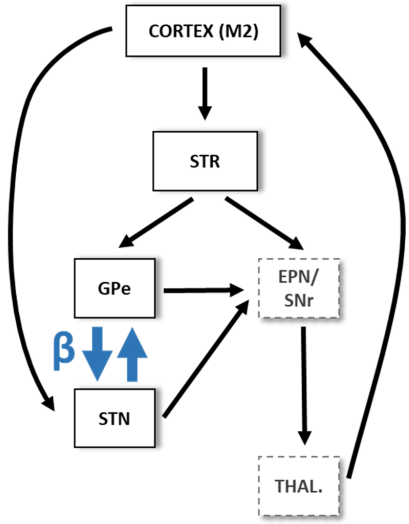	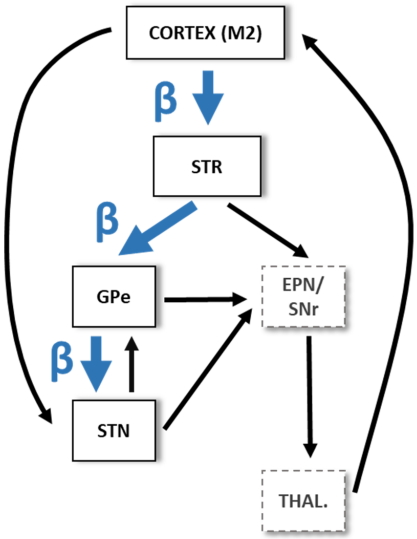
Mechanism:	**"Long-loop" resonance**	**STN/GPe Resonance Pair**	**Aberrant (cortico-) striatal output**
	Pathological beta arises from induction of a loop formed by feedback between cortex and BG	*Pathological beta arises from increased coupling of STN/GPe resonance pair.*	*Pathologica beta results from changed internal dynamics of STR and/or its outputs to the indirect pathway.*
Evidence for:	• Significant beta band STN/M2 NPD in both the forward and reverse directions. • The low beta STN → M2 feedback coherence is significantly increased in the lesioned animals. • STN/M2 NPD is undiminished by conditioning with GPe or STR.	• iCOH of the STN↔GPe suggests coupling increases in 6-OHDA experiments. • The STN→ GPe NPD its not attenuated by conditioning with the M2 ECoG.	• STN↔GPe NPDs are strongly attenuated by conditioning with STR signals. • Conditioning of the STR→ GPe NPD with the M2 ECoG is only effective in the control animals. • Conditioning of the STR→ GPe NPD with the STN LFPs is only effective in the control animals.
Evidence against:	• Conditioning the NPD with signals from the STN or M2 does not remove beta band NPD between STR and GPe, upstream of the STN. • No test to determine routing of return signal from STN to cortex.	• There is a strong asymmetry in between the forward and backwards STN↔GPe NPDs, suggesting pallidal drive is dominant. • The STN↔GPe NPDs are strongly attenuated by conditioning with the STR signal. • Conditioning NPDs with the STN signal has little effect on coupling upstream in the indirect pathway.	• Unclear whether lack of effect of conditioning is due to change in the STR output or due to change to STN signal such as that occurring due to increased hyperdirect input described in hypothesis (1).

Hypotheses for propagation of high beta/gamma rhythms

	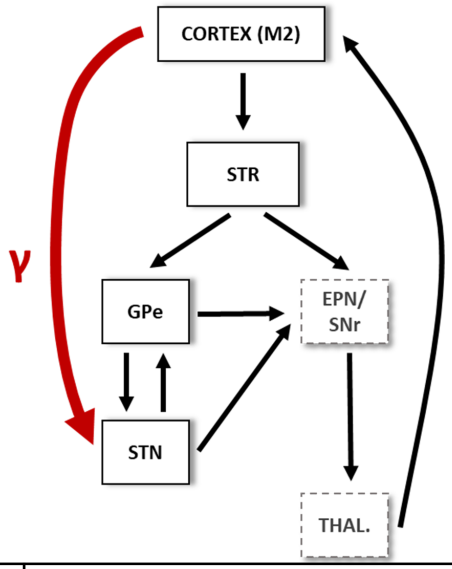	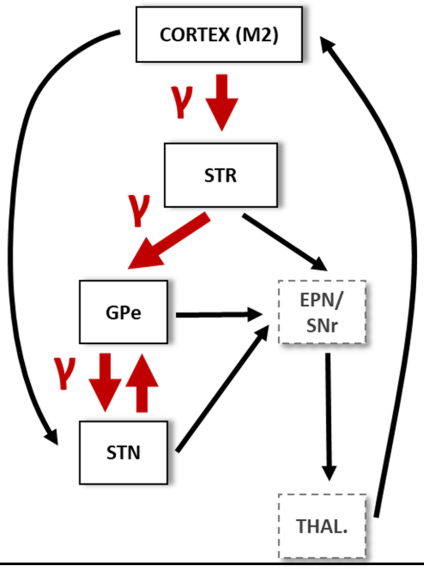	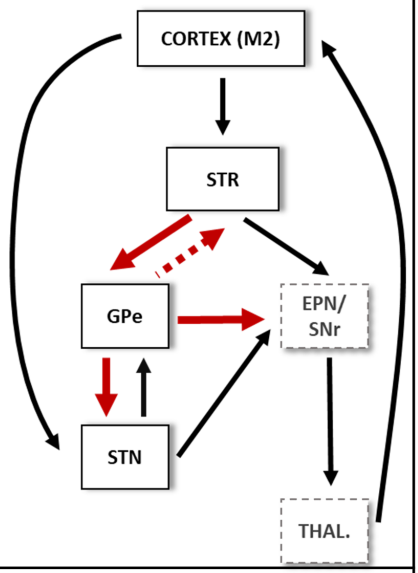
Mechanism:	**Hyper-direct inflow**	**Cortico-striatal gamma input**	**Subcortical generator**
	High beta/gamma enters the subcortical network via the hyper-direct M2→ STN connection.	*Cortical-gamma enters the BG via the striatum and is passed down the indirect pathway.*	*High beta/gamma arises from subcortical interactions and/or local dynamics within BG nuclei*
Evidence for:	• iCOH shows that M2 ↔ STR interaction is much weaker than the M2 ↔ STN. • Conditioning subcortical NPDs with ECoG attenuates a large number of connections.	• Conditioning subcortical NPDs with ECoG attenuates a large number of connections. • Conditioning of the M2 → STN NPD with STR or GPe attenuates interactions in the control condition suggesting signal is passed via striatal-pallidal projections. • NPD conditioned by the STN is less effective for interactions upstream in the indirect pathway.	• Conditioning of NPDs using signals from STR or GPe reduces strength of interactions. • Conditioning of STN→STR NPD with ECoG does not act to remove subthalamo-striatal feedback suggesting existence of subcortical feedback.
Evidence against:	• Conditioning of the M2→ STN NPD with STR or GPe signals attenuates interactions in the control conditions. •	• Conditioning of STN→STR NPD with ECoG does not act to remove subthalamo-striatal feedback suggesting existence of subcortical feedback.	• No evidence for within STR interaction from iCOH.